ULB

PUB
PRESSES UNIVERSITAIRES DE BRUXELLES

UNIVERSITÉ LIBRE DE BRUXELLES

Gravitational Waves

Compact Sources

Nicolas CHAMEL

D/2025/0098/090
1 e édition – Tirage 2024-25/1
PHYS-F-484_B

9 782500 016439

« C'est l'éducation, l'instruction qui décideront de l'émancipation de la femme et de l'homme, de leur tolérance et de leur capacité à dialoguer. »

Lucia de Brouckère (1904-1982)
Docteur en chimie de l'ULB, première femme à enseigner dans une faculté de sciences en Belgique, militante de la laïcité et du libre-examen.

NICOLAS CHAMEL

PHYS-F484

GRAVITATIONAL WAVES: COMPACT SOURCES

PUB Cours-Librairie, av. P. Héger 42, B-1000 Bruxelles / PHYS-F-484_B

Contents

These notes were written based on several textbooks[1] *and stimulating discussions with many colleagues over the past years.*

[1] Stuart L. Shapiro and Saul A. Teukolsky. *Black holes, white dwarfs and neutron stars. The physics of compact objects*. John Wiley and Sons, 1983; P. Haensel, A. Y. Potekhin, and D. G. Yakovlev. *Neutron Stars. 1. Equation of State and Structure*. Springer, New York, 2007; Michele Maggiore. *Gravitational Waves. Vol. 1: Theory and Experiments*. Oxford University Press, 2018a; Michele Maggiore. *Gravitational Waves. Vol. 2: Astrophysics and Cosmology*. Oxford University Press, 2018b; and Coleman Miller and Nicolás Yunes. *Gravitational Waves in Physics and Astrophysics: An Artisan's Guide*. Institute of Physics Publishing, 2021

1
Sources of gravitational waves

Contents

1.1 General considerations

Gravitational waves are small perturbations $h_{\mu\nu} = \delta g_{\mu\nu}$ of the background spacetime metric $\bar{g}_{\mu\nu}$ propagating at the speed of light c. They are both transverse and traceless (TT). Let us recall that the so called TT gauge (outside the source) is defined by

$$h^{0\mu} = 0\,, \qquad h^i_i = 0\,, \qquad \partial^j h_{ij} = 0\,. \tag{1.1}$$

Throughout these notes, we adopt Einstein convention. Namely summations over repeated indices are assumed

By definition, the energy flux F is the energy radiated per unit area and per unit time at a distance r from the source and is given by

$$\boxed{F = \frac{c^3}{32\pi G}\langle \dot{h}^{\rm TT}_{ij}\dot{h}^{\rm TT}_{ij}\rangle}\,, \tag{1.2}$$

where G is the constant of gravitation, the dot indicates the time derivative and $\langle . \rangle$ is the spatial average over many wave lengths or the temporal average over many periods. The luminosity L or power is the energy per unit time defined by the integration of F over the solid angle

$$L = \int d\Omega\, r^2 F\,. \tag{1.3}$$

In the linearized theory, gravitational waves are generated by time variations of the mass quadrupole moment

$$\boxed{Q_{ij} = \int d^3r\, \rho(t,\vec{r}) \left(x_i x_j - \frac{1}{3} r^2 \delta_{ij} \right)}, \tag{1.4}$$

where ρ denotes the mass-energy density. The gravitational-wave amplitude reads

$$\boxed{h_{ij}^{\rm TT}(t,\vec{r}) = \frac{1}{r} \frac{2G}{c^4} \ddot{Q}_{ij}^{\rm TT}(t - r/c)}. \tag{1.5}$$

The luminosity is given by Einstein quadrupole formula

$$\boxed{L = \frac{G}{5c^5} \langle \dddot{Q}_{ij}(t - r/c) \dddot{Q}_{ij}(t - r/c) \rangle}. \tag{1.6}$$

Gravitational waves carry away not only energy but also angular momentum at the rate given by

$$\boxed{\frac{dJ^i}{dt} = \frac{2G}{c^5} \epsilon^{ijk} \langle \ddot{Q}_{jl}(t - r/c) \dddot{Q}_{kl}(t - r/c) \rangle}. \tag{1.7}$$

1.2 *Orders of magnitude estimates*

For a source of mass m_s and size d_s varying with a characteristic frequency f_s,

$$h \sim |h_{ij}^{\rm TT}| \sim \frac{1}{r} \frac{2G}{c^4} f_s^2 m_s^2 d_s^2 = \frac{d_s}{r} \frac{\mathcal{R}_s}{d_s} \left(\frac{v_s}{c} \right)^2, \tag{1.8}$$

where $v_s = f_s d_s$ is the characteristic velocity of the source, and $\mathcal{R}_s = \dfrac{2Gm_s}{c^2}$ is the Schwarzschild radius of the source.

The flux and the luminosity are roughly given by

$$F \sim \frac{c^3}{32\pi G} h^2 f_s^2 = \frac{c^5}{32\pi G r^2} \left(\frac{\mathcal{R}_s}{d_s} \right)^2 \left(\frac{v_s}{c} \right)^6, \tag{1.9}$$

$$L = 4\pi r^2 F \sim \frac{c^5}{8G} \left(\frac{\mathcal{R}_s}{d_s} \right)^2 \left(\frac{v_s}{c} \right)^6. \tag{1.10}$$

Most important sources of gravitational waves are therefore compact $\mathcal{R}_s \sim d_s$ and relativistic $v_s \sim c$. These are white dwarfs, neutron stars and black holes. Such objects are very far, $r \gg d_s$, therefore $h \ll 1$ is very small. The gravitational-wave signal GW170817 detected by the LIGO-Virgo interferometers in 2017 was emitted by the coalescence of two neutron stars located at a distance of 40 Mpc. For comparison, the distance to the center of our galaxy is about 8 kpc

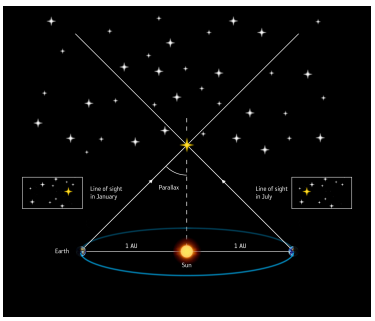

Distances of astronomical objects outside the solar system are generally measured in parsecs (pc), defined as the distance at which the parallax angle is one arcsecond. Credit: ESA.

and to the Andromeda galaxy is 0.78 Mpc. At the time GW170817 was detected, the distance between the two neutron stars was comparable with their radius. Setting $d_s \sim 10$ km and $r = 40$ Mpc, we find $h \lesssim d_s/r \sim 10^{-22}$!

However, the luminosity L of the gravitational radiation is huge because of the factor $c^5/G \approx 3.6 \times 10^{59}$ erg/s. For comparison, the electromagnetic luminosity of the Sun is $L_\odot \approx 3.8 \times 10^{33}$ erg/s, that of a typical galaxy $\sim 10^{44}$ erg/s, and that of all the galaxies in the observable Universe $\sim 10^{56}$ erg/s, i.e. still three orders of magnitude smaller than the gravitational luminosity!

The centimeter–gram–second system of units (cgs) is still widely used in astrophysics and is based on the centimeter as the unit of length, the gram as the unit of mass, and the second as the unit of time. The unit of energy is 1 erg=10^{-7} J.

1.3 *Gravitational waves from compact binary inspirals*

Gravitational-wave emission

Let us consider the inspiral of two compact objects with masses m_1 and m_2 at leading order in the post-Newtonian theory. Because gravitational waves carry away angular momentum, any eccentric orbit is circularized over the course of time. Considering a purely circular orbit, the two-body problem can be equivalently treated as an effective body with the reduced mass

$$\boxed{\mu = \frac{m_1 m_2}{m_1 + m_2}} \tag{1.11}$$

orbiting around a fixed body with mass $m = m_1 + m_2$ at a distance a.

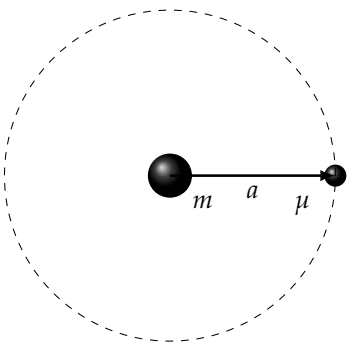

The metric perturbation $h_{ij}^{\mathrm{TT}}(t, \vec{r})$ is completely described by only two independent components. The gravitational wave amplitudes of the two polarizations at a distance r from the source are

$$h_+ = \mathcal{A}\frac{1 + \cos^2 i}{2}\cos(\omega_{\mathrm{GW}} t_{\mathrm{ret}} + 2\varphi)\,, \tag{1.12}$$

$$h_\times = \mathcal{A}\cos i \sin(\omega_{\mathrm{GW}} t_{\mathrm{ret}} + 2\varphi)\,, \tag{1.13}$$

where i is the inclination angle between the normal to the orbit and the line of sight, φ is the azimuthal angle, $\omega_{\rm GW} = 2\omega$ is the angular frequency of gravitational waves, $\omega = \dfrac{d\Phi}{dt}$ is the orbital angular frequency (Φ is the orbital phase), $t_{\rm ret} = t - r/c$ is the retarded time,

Note that gravitational waves are also emitted at frequencies other than $\omega_{\rm GW} = 2\omega$ due to higher-order mass and current multipole moments but the associated radiation is much weaker.

$$\mathcal{A} = \frac{1}{r}\frac{4G\mu\omega^2 a^2}{c^4}\,. \tag{1.14}$$

The total mass m is related to the orbital angular frequency by Kepler's law

$$\boxed{\omega^2 = \frac{Gm}{a^3}}\,. \tag{1.15}$$

Neglecting the proper motion of the source and changing the time origin, we can write $\omega_{\rm GW} t_{\rm ret} + 2\varphi = \omega_{\rm GW} t$.

- If the orbit is seen edge-on ($i = \pi/2$)

$$h_+ = \frac{\mathcal{A}}{2}\cos(\omega_{\rm GW} t)\,, \tag{1.16}$$

$$h_\times = 0\,. \tag{1.17}$$

  In the (h_+,$h_\times$) plane, the gravitational wave is described by a line: the wave is linearly polarized.

- If the orbit is seen face-on ($i = 0$)

$$h_+ = \mathcal{A}\cos(\omega_{\rm GW} t)\,, \tag{1.18}$$

$$h_\times = \mathcal{A}\sin(\omega_{\rm GW} t)\,. \tag{1.19}$$

  We thus have $h_+^2 + h_\times^2 = \mathcal{A}^2$. In the ($h_+$,$h_\times$) plane, the gravitational wave is described by a circle of radius $\mathcal{A}$: the wave is circularly polarised.

- In the general case

$$h_+ = \mathcal{A}_+\cos(\omega_{\rm GW} t)\,, \tag{1.20}$$

$$h_\times = \mathcal{A}_\times\sin(\omega_{\rm GW} t)\,, \tag{1.21}$$

  where we have introduced $\mathcal{A}_+ \equiv \mathcal{A}\dfrac{1+\cos^2 i}{2}$ and $\mathcal{A}_\times \equiv \mathcal{A}\cos i$. We thus have

$$\left(\frac{h_+}{\mathcal{A}_+}\right)^2 + \left(\frac{h_\times}{\mathcal{A}_\times}\right)^2 = 1\,. \tag{1.22}$$

  In the (h_+,$h_\times$) plane, the gravitational wave is described by an ellipse: the wave is elliptically polarized.

By measuring the polarization, it is therefore possible to constrain the inclination angle i.

Let us define the averaged characteristic gravitational-wave amplitude

$$h \equiv \sqrt{\langle h_+ \rangle^2 + \langle h_\times \rangle^2}\,. \tag{1.23}$$

Here $\langle . \rangle$ means averaging over the gravitational wave period and the spatial orientation of the orbit, i.e.

$$\langle h_+ \rangle = \frac{f_{\rm GW}}{4\pi} \int_0^{1/f_{\rm GW}} dt \int_0^{2\pi} d\varphi \int_0^{\pi} di \sin i\, h_+\,, \tag{1.24}$$

where $f_{\rm GW} = \dfrac{\omega_{\rm GW}}{2\pi}$ is the gravitational-wave frequency. Using Eqs. (1.12) and (1.13), the averaged characteristic gravitational-wave amplitude (1.23) can be written in a form similar to Eq. (1.8) with $m_s = \mu$ and $d_s = a$:

$$h = \sqrt{\frac{32}{5}} \frac{a}{r} \frac{\mathcal{R}}{a} \left(\frac{v}{c}\right)^2 . \tag{1.25}$$

where $v = a\omega$ is the orbital velocity and $\mathcal{R}_s = \dfrac{G\mu}{c^2}$ is the Schwarzschild radius associated with the effective body having the reduced mass μ.

Introducing the dimensionless post-Newtonian expansion parameter

$$\boxed{x \equiv \left(\frac{Gm\omega}{c^3}\right)^{2/3}}, \tag{1.26}$$

and the symmetric mass ratio

$$\boxed{\nu \equiv \mu/m}, \tag{1.27}$$

the averaged characteristic gravitational-wave amplitude (1.25) can be equivalently expressed as

$$h = \sqrt{\frac{32}{5}} \nu \frac{a}{r} x^2\,. \tag{1.28}$$

The luminosity is given by

$$L = \frac{32}{5} \frac{c^5}{G} \nu^2 x^5\,. \tag{1.29}$$

Let us remark that for the self-gravitating systems considered here, we have $x = \dfrac{2Gm}{ac^2} = \left(\dfrac{v}{c}\right)^2$. The symmetric mass ratio ranges from $\nu = 0$ in the test mass limit $\mu/m \to 0$ to $\nu = 1/4$ for equal mass binaries.

For a compact binary with eccentricity e with a semimajor axis a, as illustrated in the figure below, the luminosity becomes[1]

[1] P. C. Peters and J. Mathews. Gravitational Radiation from Point Masses in a Keplerian Orbit. *Physical Review*, 131(1):435–440, July 1963. DOI: 10.1103/PhysRev.131.435. URL https://doi.org/10.1103/PhysRev.131.435

$$\boxed{L = \frac{32}{5}\frac{c^5}{G}\nu^2 x^5 f(e)} \tag{1.30}$$

with

$$f(e) = \left(1-e^2\right)^{-7/2}\left(1+\frac{73}{24}e^2+\frac{37}{96}e^4\right). \tag{1.31}$$

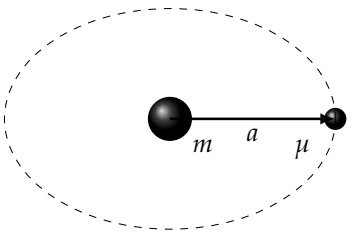

Note that $f(e) > f(0) = 1$ therefore the gravitational-wave emission is enhanced by eccentricity.

The radiation is not only emitted at angular frequency $\omega_{\rm GW} = 2\omega$, but also at different harmonics $\omega_{\rm GW} = n\omega$ with $n = 1, 2, 3, \ldots$. The peak harmonic $n_{\rm peak}$ and the corresponding frequency $f_{\rm peak}$ are approximately given by[2]

$$n_{\rm peak} \approx 2\frac{(1+e)^{1.1954}}{(1-e^2)^{3/2}}, \tag{1.32}$$

$$f_{\rm peak} \approx \frac{\sqrt{Gm}}{\pi a}\frac{(1+e)^{1.1954}}{(1-e^2)^{3/2}}. \tag{1.33}$$

[2] Linqing Wen. On the eccentricity distribution of coalescing black hole binaries driven by the kozai mechanism in globular clusters. *The Astrophysical Journal*, 598(1):419, nov 2003. DOI: 10.1086/378794. URL https://dx.doi.org/10.1086/378794

Inspiral

The emission of gravitational waves modifies the orbital motion due to the loss of energy and angular momentum. Assuming quasikeplerian orbital motion $\dot{\omega} \ll \omega^2$, the orbital frequency therefore also the gravitational-wave frequency slowly increases with time. This is referred to as "chirp". The time evolution is governed by the following equation:

$$\dot{f}_{\rm GW} = \frac{96}{5}\pi^{8/3}\left(\frac{G\mathcal{M}}{c^3}\right)^{5/3} f_{\rm GW}^{11/3} f(e), \tag{1.34}$$

where we have introduced the chirp mass

$$\boxed{\mathcal{M} \equiv \mu^{3/5} m^{2/5}}. \tag{1.35}$$

The semimajor axis a and the eccentricity e evolve according to

$$\frac{da}{dt} = -\frac{64}{5}\frac{G^3\mu m^2}{c^5 a^3} f(e), \tag{1.36}$$

$$\frac{de}{dt} = -\frac{304}{15}\frac{G^3\mu m^2}{c^5 a^4}\frac{e}{(1-e^2)^{5/2}}\left(1+\frac{121}{304}e^4\right). \tag{1.37}$$

These equations can be integrated as

$$a(e) = a_0 \frac{g(e)}{g(e_0)}\,, \tag{1.38}$$

where a_0 and e_0 are respectively the initial values of the semimajor axis and eccentricity, and

$$g(e) = \frac{e^{12/19}}{1-e^2}\left(1+\frac{121}{304}e^2\right)^{870/2299}\,. \tag{1.39}$$

The eccentricity decreases quite fast. The emission of gravitational waves circularizes the orbit long before the two objects coalesce. If $e = 0$, the orbits remain circular $\dfrac{de}{dt} = 0$ as can be seen from Eq. (1.37).

The time t_m at merger is defined as the time t at which $f_{\rm GW}(t) \to +\infty$. The time to merger $\tau = t_m - t_0$ of a binary system with a semimajor axis a_0 and eccentricity e_0 at time t_0 can be determined by integrating Eq. (1.34):

$$\boxed{\tau = \frac{5}{256}\frac{1}{(\pi f_{\rm GW})^{8/3}}\frac{c^5}{(G\mathcal{M})^{5/3}}F(e_0)} \tag{1.40}$$

with

$$F(e_0) = \frac{48}{19}\frac{1}{g(e_0)^4}\int_0^{e_0} de\frac{g(e)^4(1-e^2)^{5/2}}{e\left(1+\frac{121}{304}e^2\right)}\,. \tag{1.41}$$

Eccentricity reduces the time to merger by a factor $F(e_0) > 1$ (for a circular orbit, $F(0) = 1$).

All the expressions given so far are valid at leading post-Newtonian order (0 PN). The orbit is also found to precess with time. This effect, which appears at 1PN order, is usually referred to as periastron advance or apsidal motion, and is given by

The apsides are the orbital points farthest (apoapsis) and closest (periapsis) from the primary.

$$\dot{\psi} = \omega\frac{3G}{c^2}\frac{m}{a(1-e^2)}\,. \tag{1.42}$$

ψ is generally denoted by ω in the neutron-star literature and by γ in the white-dwarf literature. Precession can also be induced by rotations of the compact stars and their tidal interactions.

1.4 *Classes of compact objects*

The compactness of an object of mass m_s and radius R_s is characterized by the dimensionless coefficient

$$\boxed{\mathcal{C} = \frac{2Gm_s}{R_s c^2}}\,. \tag{1.43}$$

The maximum compactness $\mathcal{C}_{\max} = 1$ is achieved for black holes. For other compact stellar remnants, the compactness is limited by[3] $\mathcal{C} \leq 0.78$.

The properties of different celestial objects are summarized in Table 1.1.

	$m_s/M_\odot$	R_s (km)	ρ (g/cm^3)	$\mathcal{C}$
Earth	3×10^{-6}	6×10^3	5	10^{-10}
Sun	1	7×10^5	1	10^{-6}
white dwarfs	~ 1	10^4	$\sim 10^7$	$\sim 10^{-4}$
neutron stars	$\sim 1-2$	10	$\sim 10^{15}$	$\sim 10^{-1}$
black holes	$\gtrsim 3$	$\gtrsim 9$	0	1

Table 1.1: Main properties of different celestial objects: mass m_s in solar masses $M_\odot$, radius R_s in km, density ρ in g/cm^3, and compactness $\mathcal{C}$.

For comparison, the densest elements naturally found on Earth are osmium (22.6 g/cm^3), iridium (22.4 g/cm^3), and platinum (21.5 g/cm^3).

[3] H. Bondi. Massive spheres in general relativity. *Proceedings of the Royal Society of London. Series A, Mathematical and Physical Sciences*, 282(1390):303–317, 1964. ISSN 00804630. URL http://www.jstor.org/stable/2414776

2
White dwarfs

Contents

2.1 *The first observations of white dwarfs*

The birth of astrophysics

The end of the nineteenth century and the beginning of the twentieth were marked by the early development of astrophysics, born of the marriage of astronomy and physics. Gustav Kirchhoff and Robert Bunsen's interpretation of the absorption lines detected in the solar

spectrum by William Wollaston in 1802 and a few years later by Joseph von Fraunhofer paved the way for the spectroscopic study of the physical and chemical properties of stars. One of the most spectacular discoveries of this nascent science was the identification, against all odds, of a previously unknown chemical element thanks to the spectroscopic analysis of solar radiation by Jules Janssen and Sir Norman Lockyer. This element, named helium, was identified a few years later in radioactive ores by William Ramsay. This discovery was all the more extraordinary as probing the interior of stars seemed inconceivable just a few decades earlier. In his course on positive philosophy, Auguste Comte asserted that the chemical composition of stars was beyond the reach of human knowledge. Not only did spectroscopy allowed to probe the interior of the Sun, it also revealed a new element on Earth! This work also demonstrated the gaseous nature of stars (at least their outer layer).

The cohesion of stars could then be explained by the law of perfect gases, with the star's gravitational attraction counterbalanced by the pressure of the hot gas. But where did the heat needed to maintain equilibrium come from? Sir William Thomson (Lord Kelvin) and Hermann von Helmholtz suggested that it might come from the gravitational energy released when the star contracted. This interpretation implied an age of the Sun of only twenty million years. Yet geological studies indicated that the Earth was at least two billion years old. How could the Earth be older than the Sun? British astronomer Sir Arthur Eddington and, independently of him, French physicist Jean Perrin were among the first to glimpse the subatomic origin of stellar energy, notably following the work of chemist Francis Aston at Cambridge's Cavendish Laboratory. In 1920, Aston showed that the mass of the helium atom is less than the sum of the masses of its constituents. These measurements suggested that a great deal of energy could be contained in atomic nuclei, in accordance with Einstein's famous equation $E = mc^2$. Eddington remarked that[1] "what is possible in the Cavendish Laboratory may not be too difficult in the interior of the Sun". Eddington also stressed the importance of radiation pressure in the stability of stars. His pioneering work on the internal constitution of stars laid the foundations for stellar astrophysics[2]. In particular, he demonstrated a relationship between a star's mass and its luminosity, which was later confirmed by observations. Despite his successes, this theoretical edifice was nevertheless shaken by the discovery of white dwarfs[3].

[1] A. S. Eddington. The Internal Constitution of the Stars. *Nature.*, 106(2653):14–20, September 1920. DOI: 10.1038/106014a0. URL https://doi.org/10.1038/106014a0

[2] A. S. Eddington. *The Internal Constitution of the Stars*. Cambridge University Press, 1926

[3] A. I. Miller. *Empire of the Stars: Friendship, Obsession and Betrayal in the Quest for Black holes*. Little, Brown Book Group, 2007

The discovery of white dwarfs

The first white dwarf was discovered by the German-British astronomer Sir William Herschel in 1783, in the triple 40 Eridani system. In 1844, Friedrich Bessel predicted the existence of a companion star to Sirius in Canis Majoris and to Procyon in Canis Minoris from variations of their proper motion. These companions referred to as Sirius B and Procyon B were finally observed by Alvan Graham Clark in 1862 and John Martin Schaeberle in 1896 respectively. But the true nature of these stars was not understood until 1910 by American astronomer Henry Norris Russel, thanks to spectroscopic observations by Edward Charles Pickering and Williamina Fleming at Harvard Observatory. The spectrum of 40 Eridani B indicated a very high temperature of around ten thousand degrees. Yet 40 Eridani B was dark. In 1914, Walter Adams at the Mount Wilson Observatory in California measured the temperature of Sirius elusive partner at around 8000 K (the temperature is actually $\sim$ 27000 K). Let us recall that the temperature at the surface of the Sun is about 6000 K. Like 40 Eridani B, Sirius companion radiated very little light. In the Hertzsprung-Russel diagram of the stars' absolute magnitudes or luminosities as a function of their stellar classifications or effective temperatures, white dwarfs clearly appear as a distinct type of stars, as shown in Fig.2.1. A study of the orbits of Sirius two stars showed that Sirius B had a mass close to that of the Sun. Yet the luminosity of Sirius B was much lower than predicted by Eddington's relation. How could a star be so hot yet so dim? According to Stefan-Botzmann's law, these stars must be very small. The radius of Sirius B was estimated as 18 000 km, implying a density several tens of thousands of times greater than that of ordinary matter. For Eddington, this result was "absurd". Another white dwarf was discovered shortly afterwards by Adriaan Van Maanen. The term *white dwarf* was introduced by astronomer Willem Luyten in 1922[4] and popularized by Eddington.

At the same time, Eddington found that his mass-luminosity relationship applied not only to "giant" stars, but also to much denser "dwarf" stars like the Sun. This seemed to suggest that the interior of all stars was governed by the law of perfect gases. In 1924, he envisioned that the compression of matter in the core of a white dwarf might be possible if the temperature of the gas were high enough to strip all the electrons from the atoms. There was a way of testing this hypothesis with the theory of general relativity proposed by Einstein in 1915. Eddington was one of the most fervent supporters of this theory, and helped spread it throughout the English-speaking world. In 1919, he had led an expedition to Principe Island to test one of the predictions of Einstein's theory - the deflection of light by a gravita-

Treating the white dwarf as a black body of radius R and effective surface temperature $T_{\rm eff}$, the observed (electromagnetic) flux is given by

$$F = \frac{L}{4\pi r^2}\,, \tag{2.1}$$

where r is the distance to the white dwarf, and the luminosity follows from Stefan-Boltzman law

$$L = 4\pi R^2 \sigma T_{\rm eff}^4\,, \tag{2.2}$$

where σ is the Stefan constant. From Wien's displacement law, the effective temperature is related to the "color" of the white dwarf as determined using spectroscopy by the wavelength at the peak luminosity, $\lambda_{\rm peak} \approx \dfrac{0.3}{T_{\rm eff}}$ cm. Knowing the distance r, the radius of the white dwarf can thus be estimated as

$$R = r\sqrt{\frac{F}{\sigma T_{\rm eff}^4}}\,. \tag{2.3}$$

[4] W. J. Luyten. Third Note on Faint Early Type Stars with Large Proper Motion. *Pub. Astr. Soc. P.*, 34(202):356–357, December 1922. DOI: 10.1086/123249. URL https://doi.org/10.1086/123249

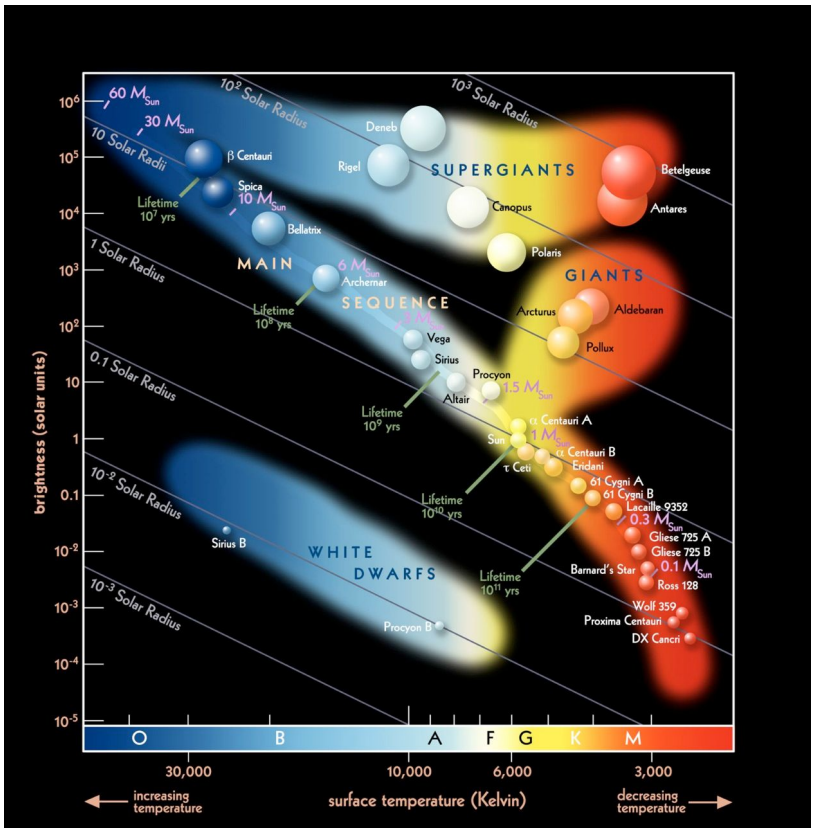

Figure 2.1: White dwarfs such as Sirius B populate a specific region of the Hertzsprung–Russell diagram: they are very faint but very hot stars.

tional field. A scientific team directed by Eddington took advantage of the total solar eclipse of May 29, 1919 to observe the stars close to the solar disk. Their positions turned out to correspond more or less to those predicted by Einstein's theory. Following this expedition, Eddington became world-famous. In 1924, he suggested applying the theory of general relativity to white dwarfs. According to this theory, if a white dwarf really was an extremely compact star, as spectroscopic observations indicated, then its intense gravitational field should lead to an observable redshift in the light emitted by the star. Walter Adams' measurement of this shift in Sirius B agreed with the value calculated by Eddington. This result not only provided further proof of Einstein's theory, but also confirmed Sirius B's prodigious density.

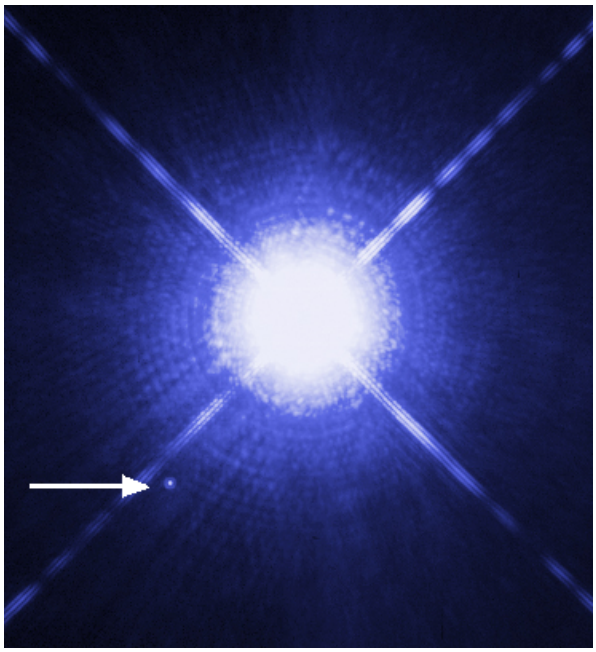

Figure 2.2: Image of Sirius A and Sirius B taken by the Hubble Space Telescope. Sirius B, which is a white dwarf, can be seen as a faint point of light to the lower left of the much brighter Sirius A. Credit: NASA/ESA/H. Bond (STScI) and M. Barstow (Univ. Leicester).

The white dwarf enigma

The global structure of a spherical white dwarf is governed by the Newtonian hydrostatic equilibrium equations

$$\frac{dP}{dr} = -\frac{Gm(r)\rho(r)}{r^2}\,, \tag{2.4}$$

where $m(r)$ is the mass enclosed in the sphere of radius r

$$m(r) = 4\pi \int_0^r dr' r'^2 \rho(r')\,. \tag{2.5}$$

The stellar radius R_s is defined by the condition $P(R_s) = 0$. The stellar mass m_s is then given by $m(R_s)$.

These equations can be readily solved for an incompressible star $\rho(r) = \rho_s$. The pressure is found to be given by

$$P(r) = \frac{2}{3}\pi G\rho_s^2(R_s^2 - r^2)\,, \tag{2.6}$$

and the mass

$$m_s = \frac{4}{3}\pi R_s^3 \rho_s\,. \tag{2.7}$$

Let us assume that the interior of a white dwarf can be described by the ideal gas law like for ordinary stars

$$P = \frac{\rho_s}{m_i} k_{\rm B} T\,, \tag{2.8}$$

where m_i is the mean mass per ion, k_B is Boltzmann constant, and T is the temperature. Subtituting Eq. (2.8) into Eq. (2.6) using Eq. (2.7) leads to the following estimate of the temperature inside the star:

$$T(r) = \frac{Gm_i m_s}{2k_B R_s}\left(1 - \frac{r^2}{R_s^2}\right) . \tag{2.9}$$

For white dwarfs, the temperature at the center is found to be of order $10^9 - 10^{10}$ K.

Eddington's paradox

Eddington observed that a white dwarf could only cool by expanding: for $T(0) \propto 1/R_s$ to decrease, R_s must increase according to Eq. (2.9). However, the expansion of the star required energy to act against gravitational attraction. A white dwarf therefore seemed doomed to inexorably collapse, a scenario Eddington deemed "absurd".

2.2 *Internal constitution of white dwarfs*

Degenerate stars

Eddington suspected that the extreme conditions prevailing in the cores of white dwarfs called for a modification of the law of perfect gases. In 1926, his colleague Ralph Fowler realized that classical mechanics itself ceased to be valid at very high density and low temperature[5]. He had the idea of applying the new quantum mechanics, one of whose founding fathers was one of his own students, the brilliant Paul Dirac. A few months earlier, Dirac and, independently, Italian physicist Enrico Fermi had discovered the statistical distribution of fermions by studying the quantization of a perfect gas. Unlike a conventional gas, the pressure of a fermion gas does not cancel out with temperature. Due to Pauli's exclusion principle, formulated in 1925, two identical particles cannot occupy the same quantum state. This results in a kind of quantum agitation of the particles. The higher the density, the greater the resulting pressure. The gas is then in a degenerate state (see Annex B).

Fowler realized that quantum mechanics could help prevent the inevitable collapse of white dwarfs, and thus resolve Eddington's paradox. He observed that matter in a white dwarf is so compressed that electrons are no longer bound to atoms even at zero temperature. He showed that electron degeneracy pressure could be sufficient to stabilize white dwarfs (since atomic nuclei are much more massive than electrons, their contribution to pressure is negligible). He pointed out that "the star is strictly analogous to one gigantic molecule in its lowest quantum state".

[5] R. H. Fowler. On dense matter. *Mon. Not. R. Astron. Soc.*, 87: 114–122, December 1926. DOI: 10.1093/mnras/87.2.114. URL https://doi.org/10.1093/mnras/87.2.114

The matter ionization does not come from the temperature as Eddington thought but from the compression induced by the gravitational pressure, as illustrated in Fig. 2.3. Indeed, at high enough densities the interatomic spacing given by $(3/(4\pi n_N))^{1/3}$ becomes comparable to the atomic radius $\sim a_0/Z^{1/3}$, where n_N is the number density of atoms and a_0 is the Bohr radius (see Annex A). Considering matter containing elements with atomic number Z and mass number A, this occurs when $n_N \sim 3Z/(4\pi a_0^3)$. The mass density ρ is mainly determined by atomic nuclei (the electron mass m_e is much smaller than the proton mass m_p). Approximating the atomic mass by $m_N \approx Am_p$ (the mass is actually slightly lower due to the nuclear binding energy), the ionization density is thus given by

$$\rho_i \sim \frac{3}{4\pi} AZ \frac{m_p}{a_0^3} \approx 3AZ \text{ g cm}^{-3}. \tag{2.10}$$

At densities $\rho \gg \rho_i$, atoms are crushed into a dense plasma of nuclei and free electrons. Because of electric charge neutrality, the electron number density is given by $n_e = Zn_N$. Depending on the temperature, nuclei can be in a liquid or solid state. Electrons on the other hand are highly degenerate and behave as a cold Fermi gas. Indeed, the electron Fermi temperature defined by $T_{Fe} = \varepsilon_{Fe}/k_B$, where $\varepsilon_{Fe} = \dfrac{\hbar^2 k_{Fe}^2}{2m_e}$ is the electron Fermi energy with $k_{Fe} = (3\pi^2 n_e)^{1/3}$ the Fermi wave number, can be estimated as

$$T_{Fe} \approx 3.1 \times 10^9 \left(\frac{Z}{A}\right)^{2/3} \left(\frac{\rho}{10^6 \text{ g cm}^{-3}}\right)^{2/3} \text{K}. \tag{2.11}$$

This is much higher than the temperature of order $10^6 - 10^7$ K expected in white dwarfs, as inferred from their observed luminosity. Electrons provide the main contribution to the pressure

$$P \approx P_e = \frac{(3\pi^2)^{2/3}\hbar^2}{5m_e m_p^{5/3}} \left(\frac{Z}{A}\right)^{5/3} \rho^{5/3}. \tag{2.12}$$

Note that ions are not degenerate. This is because they are much more massive than electrons. Their Fermi temperature is much lower,

$$T_{Fi} \approx \frac{1.6 \times 10^6}{A^{5/3}} \left(\frac{\rho}{10^6 \text{ g cm}^{-3}}\right)^{2/3} \text{K}.$$

For $A \approx 10$ and $\rho \approx 10^6$ g cm^{-3}, $T_{Fi} \approx 3 \times 10^4$ K.

Limiting density and mass-radius relation

In 1929, physicist Edmund Clifton Stoner from Leeds University investigated the effect of electron degeneracy on the structure of a white dwarf using heuristic arguments[6] (Stoner, who was a student of Rutherford at Cambridge, is best known for his work on ferromagnetism). To simplify calculations, Stoner treated the interior of a white dwarf as an incompressible sphere of radius R_s and density ρ_s. Instead of solving the hydrostatic equilibrium equations (2.4) and (2.5), he determined the global structure a white dwarf with a

[6] Edmund C. Stoner. V. the limiting density in white dwarf stars. *The London, Edinburgh, and Dublin Philosophical Magazine and Journal of Science*, 7(41):63–70, 1929. DOI: 10.1080/14786440108564713. URL https://doi.org/10.1080/14786440108564713

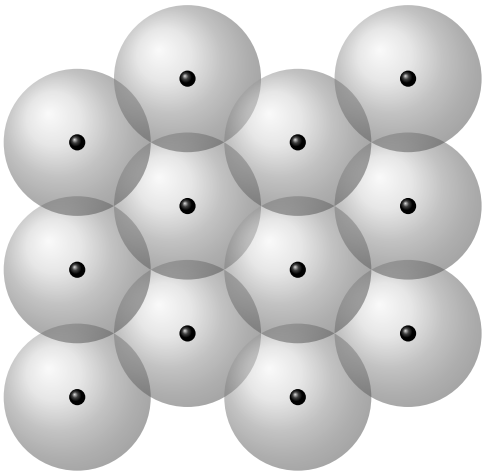

Figure 2.3: Schematic picture of matter ionization in the core of a white dwarf

given mass $m_s = \frac{4}{3}\pi R_s^3 \rho_s$ from the minimization of the total energy $E = E_{\rm int} + E_{\rm grav}$, where the first term accounts for the internal energy of the electron gas

$$E_{\rm int} = \frac{4}{3}\pi R_s^3 \mathcal{E}_e \,, \tag{2.13}$$

whereas the second term is the gravitational energy

$$E_{\rm grav} = -\frac{3}{5}\frac{G m_s^2}{R_s} \,. \tag{2.14}$$

Here $\mathcal{E}_e$ denotes the electron energy density given by (see Annex B)

$$\mathcal{E}_e = \frac{\hbar^2 k_{Fe}^5}{10\pi^2 m_e} \,. \tag{2.15}$$

Stoner thus obtained the limiting density

$$\rho_s = \frac{256\pi^3}{27}\frac{G^3}{h^6} m_e^3 m_p^5 \left(\frac{A}{Z}\right)^5 m_s^2 \approx 4\times 10^4 \left(\frac{A}{Z}\right)^5 \left(\frac{m_s}{M_\odot}\right)^2 \text{ g cm}^{-3} \,. \tag{2.16}$$

Eliminating ρ_s leads to a relation between the mass and the radius of a white dwarf

$$\left(\frac{R_\oplus}{R_s}\right)^3 \approx 2.2\times 10^{-2} \left(\frac{A}{Z}\right)^5 \frac{m_s}{M_\odot} \,, \tag{2.17}$$

where we have introduced the Earth radius $R_\oplus \approx 6400$ km. Unlike ordinary stars, the more massive a white dwarf is, the smaller it is.

Special relativity and maximum mass

Wilhelm Anderson of the University of Tartu in Estonia pointed out to Stoner that electrons in the core of a white dwarf could have

speeds close to the speed of light[7]. Indeed, using Eq. (2.16), the electron Fermi velocity $v_{Fe} = \dfrac{\hbar k_{Fe}}{m_e}$ inside a white dwarf is given by

$$\frac{v_{Fe}}{c} \approx 3.4 \times 10^{-1} \left(\frac{A}{Z}\right)^{4/3} \left(\frac{m_s}{M_\odot}\right)^{2/3} . \tag{2.18}$$

According to Einstein's theory of special relativity, no particle can move faster than light. Anderson realized that special relativity limited the quantum agitation of electrons at very high density and therefore reduced their resistance to the star's gravitational collapse. He realized that a white dwarf could not be stable beyond a certain critical mass, which he roughly estimated as $0.69 M_\odot$ assuming $A/Z = 5/2$ (roughly the ratio for lead - note that with a density of 11 g cm^{-3} lead is not the densest element on Earth). This limiting mass was lower than the estimated mass of Sirius B. Stoner improved Anderson's approximate treatment considering an ultrarelativistic gas of electrons for which the energy density is given by (see Annex B)

$$\mathcal{E}_e = \frac{\hbar c k_{Fe}}{4\pi^2} . \tag{2.19}$$

Following the same line of reasoning as before, he found that an equilibrium solution only exists if $m_s < m_{\rm Stoner}$, where[8]

$$\boxed{m_{\rm Stoner} = \frac{15\sqrt{5\pi}}{16} \left(\frac{Z}{A}\right)^2 \left(\frac{\hbar c}{G}\right)^{3/2} \frac{1}{m_p^2}} . \tag{2.20}$$

For $A/Z = 5/2$, this yields $m_{\rm Stoner} \approx 1.1 M_\odot$. But neither Anderson nor Stoner discussed about the implications of their results.

Chandrasekhar limit

In 1930, a talented young Indian student Subrahmanyan Chandrasekhar had won a scholarship from the Indian government to study in England. Chandrasekhar was eager to work on the structure of white dwarfs with Fowler at Cambridge. In the summer of 1930, aboard the Lloyd Triestino liner taking him to Europe, Chandrasekhar also understood that special relativity could bring important modifications to Fowler's results on the properties of a degenerate electron gas. Although his work was not published until 1931[9] after those of Stoner and Anderson (of which he was unaware until his arrival at Cambridge), Chandrasekhar's treatment of the structure of a white dwarf was far more realistic.

After calculating the pressure of an electron Fermi gas in the high-density regime, Chandrasekhar solved the equations (2.4) and (2.5) for the hydrostatic equilibrium of a white dwarf whose constituting

[7] Wilhelm Anderson. Über die Grenzdichte der Materie und der Energie. *Zeitschrift fur Physik*, 56 (11-12):851–856, November 1929. DOI: 10.1007/BF01340146. URL https://doi.org/10.1007/BF01340146

[8] Edmund C. Stoner. Lxxxvii. the equilibrium of dense stars. *The London, Edinburgh, and Dublin Philosophical Magazine and Journal of Science*, 9(60):944–963, 1930. DOI: 10.1080/14786443008565066. URL https://doi.org/10.1080/14786443008565066

[9] S. Chandrasekhar. The Maximum Mass of Ideal White Dwarfs. *Astrophys. J.*, 74: 81, July 1931. DOI: 10.1086/143324. URL https://doi.org/10.1086/143324

matter is described by a polytropic equation of state of the form $P = K\rho^\gamma$, where $\gamma = 1 + \frac{1}{n}$ is the adiabatic index and n is the polytropic index.

Figure 2.4: Portrait of a young Subrahmanyan Chandrasekhar as Fellow of Trinity College, Cambridge in 1934. AIP Emilio Segrè Visual Archives.

Introducing the dimensionless variables $x = r/r_0$ and $y = \left(\frac{\rho}{\rho_c}\right)^{1/n}$, where $\rho_c = \rho(r=0)$ and

$$r_0 = \sqrt{\frac{K}{4\pi G}\frac{\gamma}{\gamma-1}\rho_c^{\gamma-2}}, \tag{2.21}$$

the hydrostatic equilibrium equation (2.4) can be recast into the Lane-Emden equation

$$\frac{d}{dx}x^2\frac{dy}{dx} = -x^2y^n\,, \tag{2.22}$$

with the conditions $y(0) = 1$ and $y'(0) = 0$.

Analytic solutions are known for specific values of n. For $n < 5$, the function $y(x)$ vanishes for some finite value of $x = x_n$ thus defining the radius of the star through

$$R_s = r_0 x_n = x_n\sqrt{\frac{K}{4\pi G}\frac{\gamma}{\gamma-1}\rho_c^{\gamma-2}}\,. \tag{2.23}$$

The mass of the star is then obtained from Eq. (2.5) and can be expressed as

$$m_s = \frac{1}{\sqrt{4\pi}} \left(\frac{\gamma}{\gamma - 1} \frac{K}{G} \right)^{3/2} \rho_c^{\frac{3\gamma-4}{2}} (-x_n y'(x_n)) \,. \tag{2.24}$$

Comparing Eqs. (2.23) and (2.24), it can be easily seen that $m_s^{\gamma-2} \propto R_s^{3\gamma-4}$.

Considering ultrarelativistic electrons, the equation of state takes a polytropic form with $n = 3$:

$$P \approx \frac{\hbar c (3\pi^2)^{1/3}}{4} \left(\frac{Z}{A m_p} \right)^{4/3} \rho^{4/3} \,. \tag{2.25}$$

Remarkably, the mass becomes independent of the radius:

$$m_s = \frac{1}{\sqrt{4\pi}} \left(\frac{4K}{G} \right)^{3/2} (-x_3^2 y'(x_3)) \,, \tag{2.26}$$

$$R_s = \sqrt{\frac{K}{\pi G}} \frac{x_3}{\rho_c^{1/3}} \,. \tag{2.27}$$

Using the known solution of the Lane-Emden equation, $x_3 \approx 6.89685$ and $x_3^2 y'(x_3) = -2.01824$ yields

$$\boxed{m_{\rm Ch} = 3.09798 \left(\frac{Z}{A} \right)^2 \left(\frac{\hbar c}{G} \right)^{3/2} \frac{1}{m_p^2}} \,. \tag{2.28}$$

Substituting $A/Z = 5/2$, Chandrasekhar found $m_{\rm Ch} \approx 0.91 M_\odot$. The limiting mass he obtained differed by less than 20% from that calculated by Stoner.

The existence of a mass limit was independently demonstrated by Soviet theoretical physicist Lev Landau[9] in 1931 but his work was published only in 1932[10]. Landau's formulation was more general and elegant. It revealed the four fundamental constants: the gravitational constant G, the mass of the proton m_p, Planck's constant h and the speed of light c, thus highlighting the role of quantum mechanics and special relativity. His numerical estimate was also more realistic as he considered $A/Z = 2$ instead of $5/2 = 2.5$, as expected since white dwarfs are composed mainly of carbon and oxygen. However, Landau did not believe that a white dwarf whose mass exceeded the critical mass would collapse. To avoid this "ridiculous" eventuality, he proposed: "we must conclude that more massive stars possess regions within which quantum mechanics is violated"!

In 1932, Stoner obtained an expression for the pressure of a degenerate electron gas valid for all densities[11]. In a seminal paper published in 1928, physicist Yakov Frenkel had already calculated the

[10] L. D. Landau. To the Stars theory. *Phys. Zs. Sowjet*, 1:285, December 1932

[11] E. C. Stoner. The minimum pressure of a degenerate electron gas. *Monthly Notices of the Royal Astronomical Society*, 92(7):651–661, 05 1932. ISSN 0035-8711. DOI: 10.1093/mnras/92.7.651. URL https://doi.org/10.1093/mnras/92.7.651

pressure of degenerate matter, taking into account the interactions between electrons and atomic nuclei. But his work was long ignored by the scientific community[12]. Following the advice of Armenian astrophysicist Victor Ambarstoumian, whom he met in Leningrad in July 1934, Chandrasekhar used Stoner's results to calculate the structure of white dwarfs of different masses. In particular, he showed that approaching the mass limit (2.26), the radius of the star tends towards zero, while the density becomes infinitely large as can be seen from Eq. (2.27). His work implied that a white dwarf whose mass exceeds the mass limit would then collapse.

[12] Dmitrii G. Yakovlev. From the history of physics: The article by Ya I Frenkel' on 'binding forces' and the theory of white dwarfs. *Physics Uspekhi*, 37(6):609–612, June 1994. DOI: 10.1070/PU1994v037n06ABEH000031. URL https://doi.org/10.1070/PU1994v037n06ABEH000031

Many physicists and astrophysicists, including Einstein and Eddington, refused to accept such a scenario. On January 11, 1935, at a meeting of the Royal Astronomical Society at Burlington House, Eddington, then at the height of his fame, refuted Chandrasekhar's work on white dwarfs. Eddington humiliated the young Indian, claiming that his results did not correspond to physical reality. Eddington had been engaged for some years in developing his own fundamental theory, the keystone of which was the impossibility of neglecting interactions between particles. Chandrasekhar's calculations assumed a gas of electrons with no interactions. Eddington went so far as to question the application of special relativity to quantum mechanics (implying the existence of a mass limit for white dwarfs), despite Dirac's work, for which he had been awarded the Nobel Prize in Physics two years earlier. Chandrasekhar received support from leading physicists such as Niels Bohr and Wolfgang Pauli, but the latter refused to publicly contradict Eddington, who enjoyed an immense reputation at the time. In 1936, Chandrasekhar left England for the USA, where he remained until his death in 1995. One of the main architects of the white dwarf theory, Chandrasekhar was awarded the Nobel Prize in Physics in 1983.

Matter neutronization

Chandrasekhar's work had led to the revolutionary conclusion that a white dwarf whose mass exceeded the mass limit must collapse in a point of infinite density. More precisely, he showed that the maximum mass was reached in the limit of ultrarelativistic electrons, when the dimensionless ratio $\frac{p_{Fe}}{m_e c} \to +\infty$. This limit can be equivalently written as $\frac{\rho}{\rho_{\rm rel}} \to +\infty$ with

$$\rho_{\rm rel} \equiv \frac{1}{3\pi^2}\frac{A}{Z}\frac{m_p}{\lambda_e^3} \approx 10^6 \frac{A}{Z}\ {\rm g\ cm^{-3}}\,, \tag{2.29}$$

where $\lambda_e = \frac{\hbar}{m_e c}$ is the electron Compton wavelength.

However, it is clear that the equation of state (2.25) cannot be applied to arbitrarily high densities. At some point, nuclei will become close enough to each other that their contribution to the pressure will no longer be negligible. Nevertheless, knowledge of nuclear physics remained rudimentary. Since Sir Ernest Rutherford's discovery of the atomic nucleus in 1911, little progress had been made. An atom was assumed to consist of an electrically neutral set of electrons orbiting a much more massive central nucleus, like the planets of the solar system orbiting the Sun. Rutherford thought that the nucleus itself was constituted of "positive electrons", which he called "protons", whose electrical charge was exactly the opposite of that of an electron. He imagined that some electrons must have collapsed onto the nucleus to explain the difference between the atomic number of nuclei and their number of charges (the latter being determined by the number of orbiting electrons). In 1920, Rutherford speculated on the possible existence of a nucleus with atomic number unity but zero charge number, formed by a proton combined with an electron. The word "neutron" was attributed to Rutherford by one of his disciples, Glasson, in 1921. Nevertheless, the origin of the word is much older[13]. Dmitri Medeleev's work on classifying elements by their chemical properties also led to the postulation of the existence of a hypothetical "neutronium". In the 1920s, Rutherford and his team at the Cavendish Laboratory in Cambridge carried out several experiments in an attempt to identify this new particle, but without success. In 1930, German physicists Walther Bothe and Herbert Becker discovered ultra-penetrating but non-ionizing radiation by bombarding beryllium with helium nuclei. In January 1932, Frédéric and Irène Joliot-Curie demonstrated that this new type of radiation was capable of ejecting protons from a paraffine wax target. They assumed that this radiation was electromagnetic in origin, by analogy with the photoelectric effect in metals. A Rutherford assistant named James Chadwick showed that this radiation could not be electromagnetic in origin, and immediately realized that it could be neutrons. He conducted a series of experiments to confirm their existence, and announced his discovery in February 1932. Two years later, he and Maurice Goldhaber devised an experiment to measure the mass of the neutron. The interpretation of the neutron as an electron collapsed onto a proton gradually disappeared, particularly following the publication of Enrico Fermi's theory of beta radioactivity in 1934. It became increasingly clear that the neutron was a particle in its own right. In 1935, Chadwick was awarded the Nobel Prize in Physics for this momentous discovery, which revolutionized not only nuclear physics, but also stellar astrophysics.

Soon after the discovery of the neutron, it was realized that matter

[13] Abraham Pais. *Inward bound. Of matter and forces in the physical world*. Oxford University Press, 1986

becomes more and more neutron rich at high densities. In vacuum, a neutron is unstable and decays into protons because $m_n > m_p$ (the energy $m_n c^2$ of a neutron star is higher than that $m_p c^2$ of a proton). However, neutrons can be stable in dense matter due to the capture of electrons by nuclei:

$$(A, Z) + e^- \to (A, Z-1) + \nu_e \,. \tag{2.30}$$

Ignoring electron-ion interactions and the neutrino mass, this reaction becomes energetically allowed if the electron Fermi energy ε_{Fe} exceeds some threshold value determined by the condition

$$M(A, Z)c^2 + \varepsilon_{Fe} > M(A, Z-1)c^2 \,. \tag{2.31}$$

Approximating the nuclear mass by $M(A, Z) \approx (A - Z)m_n + Zm_p$, Eq. (2.31) reduces to

$$\varepsilon_{Fe} > \varepsilon_\beta \equiv (m_n - m_p)c^2 \,. \tag{2.32}$$

Considering ultrarelativistic electrons, $\varepsilon_{Fe} \approx \hbar c(3\pi^2 n_e)^{1/3}$, leads to $\rho > \rho_\beta$ with

$$\rho_\beta = \frac{1}{3\pi^2}\frac{A}{Z} m_p \left(\frac{\varepsilon_\beta}{\hbar c}\right)^3 \approx 1.6 \times 10^7 \frac{A}{Z} \text{ g cm}^{-3} \,. \tag{2.33}$$

Note that $\rho_\beta \gg \rho_{\rm rel}$ and this justifies our assumption of ultrarelativistic electrons.

In 1956, the French physicist Evry Schatzman[14] showed that the central density of white dwarfs is limited by the onset of electron captures by nuclei, implying that the radius of the most massive white dwarfs remains finite. From Eq. (2.27), the minimum radius is given by

$$R_{\rm min} = \frac{K}{\pi G}\frac{x_3}{\rho_\beta^{1/3}} \,. \tag{2.34}$$

The stability of a white dwarf can be further limited by general relativity, as was first shown by Kaplan[15].

Detailed calculations of the structure of white dwarfs taking into account matter neutronization were performed at the end of the 1950's and at the beginning of the 1960's.

[14] E. Schatzman. Influence of the Nucleon-Electron Equilibrium on the Internal Structure of White Dwarfs. *Astronomiceskij Zhurnal*, 1956; and Evry Schatzman. *White Dwarfs*. North-Holland Publishing Company, 1958

[15] S. A. Kaplan. Sverkhplotnyè Zvezdy. *Naukovy Zapiski*, 15:109–115, 1949

2.3 *Formation and classification of white dwarfs*

Stellar evolution

An ordinary star spends most of its life burning hydrogen into helium. This stage depends on the star's mass m_s and lasts about

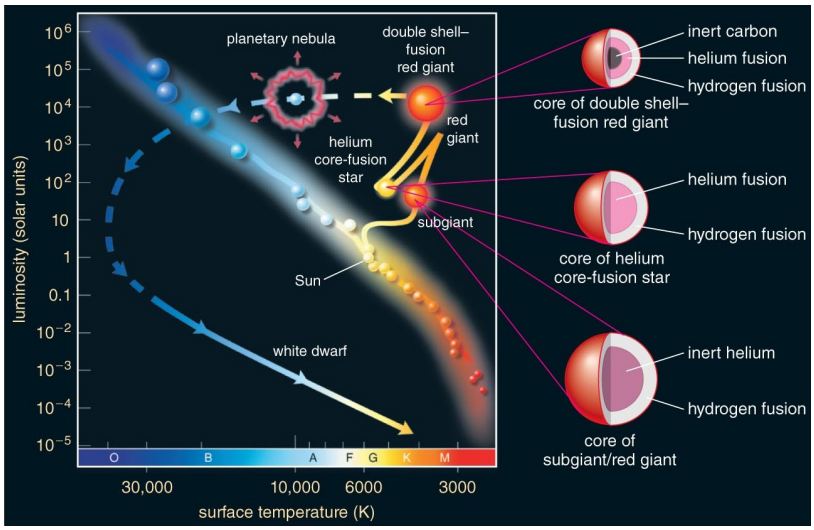

Figure 2.5: Evolution of a main sequence star comparable to the Sun into a white dwarf. From Bennett et al. 2017.

$\sim 7.3 \times 10^9 \left(\frac{M_\odot}{m_s}\right)^{5/2}$ years. Stars of different masses lie on the so called main sequence in the Hertzsprung-Russell diagram, see Fig. 2.1. The subsequent evolution of stars is dictated by their mass.

White dwarfs are the remnants of stars, whose mass on the main sequence was less than about $8M_\odot$ (90% of the stars). The different stellar evolution stages are illustrated in Fig. 2.5. The burning of hydrogen stops when the mass fraction of helium exceeds about 12%. Due to the lack of thermal pressure, the core collapses and heats up. This triggers hydrogen burning in the envelope, which expands and cools down. The luminosity of the star increases by several orders of magnitude. The star leaves the main sequence and becomes a red giant. When the temperature T of the core attains about 10^8 K, the fusion of helium into carbon and oxygen opens. The inert stellar core remains relatively cold and supported by the electron degeneracy pressure since $T \ll T_{Fe}$ (compare with Eq. (2.11)). Therefore, the core continues to heat up thus increasing further the fusion reactions, which become unstable. This leads to the so called helium flash. As T reaches T_{Fe}, the degeneracy is raised and the pressure now increases with T: the star expands and cools down thus stabilizing helium burning. Once helium in the core is exhausted, the burning proceeds in the helium envelope: the star is on the asymptotic giant branch. At some point, the star enters an unstable phase and loses some of its hydrogen envelope. The star contracts thus increasing the effective surface temperature. The emitted radiation is shifted towards the ultraviolet and ionizes the ejected envelope: this is observed as a planetary nebula. Once the mass of the hydrogen envelope decreases

below $10^{-4}M_\odot$, the reactions stop and the star becomes a white dwarf. Main-sequence stars with a mass $8-10M_\odot$ may be sufficiently massive to burn carbon into neon and magnesium leading to oxygen-neon-magnesium white dwarfs. Initially very hot with effective surface temperatures of order 10^5 K, white dwarfs cool down very slowly during billions of years. The cooling is temporarily slowed down when the core crystallizes due to the release of latent heat.

Classification

White dwarfs are identified by the letter D (degenerate stars) followed by a sequence of letters specifying their spectral type and features.

Spectral types:

A	H lines present
B	He I lines
C	Continuous spectrum; no lines
O	He II lines, accompanied by He I or H lines
Z	Ca II, Mg, Fe, Si lines
Q	Carbon lines present
X	Unclassifiable spectrum

Peculiar features:

P	Magnetic white dwarf with detectable polarization
H	Magnetic white dwarf without detectable polarization
E	Emission lines present
V	Variable

The number of known white dwarfs has increased dramatically with the data collected by the Gaia mapping of our galaxy, as shown in Table 2.1.

1926	1939	1950	1999	2018	2021
4	18	~ 100	2000	~ 260000	~ 359000

Table 2.1: Number of known white dwarfs (including candidates) at different times.

2.4 *White dwarfs as gravitational wave sources*

Indirect observations of gravitational-wave emission

Electromagnetic observations of short-period binary white dwarfs provide indirect confirmation of the emission of gravitational waves.

In particular, SDSS J0651+2844 is a binary with an orbital period $P_{\rm orb}$ of 12.75 minutes[16]. The binary is detached meaning that mass transfer is negligible. The decay of the orbital period was estimated as $\dot{P}_{\rm orb} = -0.31 \pm 0.09$ ms/yr by measuring times between eclipses.

[16] J. J. Hermes et al. Rapid Orbital Decay in the 12.75-minute Binary White Dwarf J0651+2844. *Astrophys. J. Lett.*, 757(2): L21, October 2012. DOI: 10.1088/2041-8205/757/2/L21. URL https://doi.org/10.1088/2041-8205/757/2/L21

The white dwarfs masses could be extracted from the fit of the observed light curves: $m_1 = 0.26 \pm 0.04 M_\odot$ and $m_2 = 0.5 \pm 0.04 M_\odot$.

Using Eq. (1.34) and assuming quasicircular orbits, the variation of the orbital period due to the emission of gravitational waves at frequency $f_{\rm GW} = \dfrac{2}{P_{\rm orb}}$ is given by

$$\dot{P}_{\rm orb} = -(2\pi)^{8/3} \frac{96}{5} \left(\frac{G\mathcal{M}}{P_{\rm orb} c^3} \right)^{5/3} . \tag{2.35}$$

Substituting the measured values of the masses and orbital period yields $\dot{P}_{\rm orb} = -0.26$ ms/yr in good agreement with observations.

A few such short-period binary white dwarfs are known and will be verification sources for future gravitational-wave detectors[17].

[17] Eliot Finch et al. Identifying LISA verification binaries among the Galactic population of double white dwarfs. *Monthly Notices of the Royal Astronomical Society*, 522(4):5358–5373, 04 2023. ISSN 0035-8711. DOI: 10.1093/mnras/stad1288. URL https://doi.org/10.1093/mnras/stad1288

Future observations with space-based detectors

White dwarfs are not currently detectable by ground-based interferometers but white dwarf binaries will be primary targets of space-based detectors such as the Laser Interferometer Space Antenna (LISA).

The lowest accessible gravitational-wave frequencies with LISA will be ~ 1 mHz. Considering the quasicircular inspiral of two white dwarfs to leading order in post Newtonian theory, this corresponds to an orbital period $P_{\rm orb} = \dfrac{2}{f_{\rm GW}}$ of about 17 minutes and to an orbital distance $a = \left(\dfrac{Gm}{\pi^2 f_{\rm GW}^2} \right)^{1/3}$ of about 2.5×10^5 km for typical white dwarf masses $m_1 = m_2 = 0.6 M_\odot$. White dwarfs will thus still be very far apart (recalling that their typical radius is about $10^3 - 10^4$ km) and can be treated as point like to a very good approximation.

The expected gravitational-wave amplitude can be estimated as

$$\mathcal{A} \approx 1.18 \times 10^{-22} \left(\frac{\mathcal{M}}{0.25 M_\odot} \right)^{5/3} \left(\frac{f_{\rm GW}}{1 \text{ mHz}} \right)^{2/3} \left(\frac{1 \text{ kpc}}{r} \right) . \tag{2.36}$$

For $f_{\rm GW} \lesssim 2$ mHz, binary white dwarfs will form an unresolved foreground. Among the $\sim 10^8$ white dwarf binaries present in our Galaxy, $\sim 10^4$ will be detectable (above the noise).

For quasicircular compact binary inspiral ($\dot{\omega} \ll \omega^2$), the time evolution of the gravitational-wave frequency is dictated by Eq. (1.34)

$$\dot{f}_{\rm GW} \approx 1.81 \times 10^{-11} \left(\frac{\mathcal{M}}{0.25 M_\odot} \right)^{5/3} \left(\frac{f_{\rm GW}}{1 \text{mHz}} \right)^{11/3} \text{Hz yr}^{-1} . \tag{2.37}$$

The time τ to merger (1.40) can be estimated as

$$\tau \approx 20.6 \left(\frac{0.25 M_\odot}{\mathcal{M}} \right)^{5/3} \left(\frac{1 \text{mHz}}{f_{\rm GW}} \right)^{8/3} \text{Myrs} . \tag{2.38}$$

LISA will therefore be able to observe binary white dwarfs millions of years before their merger.

After the four year duration of the LISA mission, the variation of $f_{\rm GW}$ will thus be of order $\delta f_{\rm GW} \sim 10^{-11} - 10^{-10}$Hz $\ll f_{\rm GW}$: binary white dwarfs will be observed as quasimonochromatic sources. Still, LISA should be able to measure $\dot{f}_{\rm GW}$, thus allowing to extract the chirp mass

$$\mathcal{M} = \frac{c^3}{G}\left(\frac{5}{96}\right)^{3/5} \frac{1}{\pi^{8/5}} \dot{f}_{\rm GW}^{3/5} f_{\rm GW}^{-11/5}. \tag{2.39}$$

If the frequency is high enough ($f_{\rm GW} \gtrsim 10^{-2}$ Hz), it could also be possible to measure $\ddot{f}_{\rm GW}$ and to extract some information about the internal structure of white dwarfs (higher frequencies means that the white dwarfs are closer).

Some of the observed binaries will be highly eccentric and these systems could potentially provide more information on the constitution of white dwarfs[18]. Precession leads to a splitting of each harmonic $nf_{\rm GW}$ into a triplet with frequencies $nf_{\rm GW}$ and $nf_{\rm GW} \pm \frac{\dot{\psi}}{\pi}$, where $\dot{\psi}$ denotes the advance of the periastron. For typical binary white dwarfs eccentricity $e \lesssim 0.5$, the amplitudes of the gravitational signals with frequencies $nf_{\rm GW} - \frac{\dot{\psi}}{\pi}$ and $nf_{\rm GW}$ will be negligible, and only the frequencies $nf_{\rm GW} + \frac{\dot{\psi}}{\pi}$ will thus be detected by LISA. For $f_{\rm GW} \gtrsim 1$ mHz, it will be possible to measure $\dot{\psi}$ with an error of $1 - 10\%$ using LISA. Assuming that the orbital and rotation periods are long compared to the oscillation periods of the white dwarfs (no resonance), the advance of the periastron can be decomposed into three different contributions:

$$\dot{\psi} = \dot{\psi}_{\rm GR} + \dot{\psi}_{\rm rot} + \dot{\psi}_{\rm tides}\,, \tag{2.40}$$

where $\dot{\psi}_{\rm GR}$ given by Eq. (1.42) is due to general relativity, while the last two terms account for quadrupolar distorsions of white dwarfs induced by centrifugal and tidal forces, and are given by

$$\dot{\psi}_{\rm rot} = \left(\frac{R_1}{a}\right)^5 \frac{m}{m_1}\frac{\omega_1}{(1-e^2)^2}k_{2,1} + \left(\frac{R_2}{a}\right)^5 \frac{m}{m_2}\frac{\omega_2}{(1-e^2)^2}k_{2,2}\,, \tag{2.41}$$

$$\dot{\psi}_{\rm tides} = 15\omega \frac{1+\frac{3}{2}e^2+\frac{1}{8}e^4}{(1-e^2)^5}\left[\left(\frac{R_1}{a}\right)^5 \frac{m_2}{m_1}k_{2,1} + \left(\frac{R_2}{a}\right)^5 \frac{m_1}{m_2}k_{2,2}\right]. \tag{2.42}$$

Here ω_1 and ω_2 are the spin angular velocities of the two white dwarfs of radius R_1 and R_2 respectively. The rotations of the white dwarfs can be supposed to be synchronized with the orbital motion[19]

[18] F. Valsecchi, W. M. Farr, B. Willems, C. J. Deloye, and V. Kalogera. Tidally Induced Apsidal Precession in Double White Dwarfs: A New Mass Measurement Tool with LISA. *Astrophys. J.*, 745(2):137, February 2012. DOI: 10.1088/0004-637X/745/2/137. URL https://doi.org/10.1088/0004-637X/745/2/137

[19] Jim Fuller and Dong Lai. Dynamical tides in compact white dwarf binaries: tidal synchronization and dissipation. *Mon. Not. R. Astron. Soc.*, 421(1):426–445, March 2012. DOI: 10.1111/j.1365-2966.2011.20320.x. URL https://doi.org/10.1111/j.1365-2966.2011.20320.x

for orbital periods $\lesssim 45-130$ minutes therefore $\omega_1 \approx \omega_2 \approx \omega$. The dimensionless coefficients $k_{2,1}$ and $k_{2,2}$ are so called Love numbers and characterize the quadrupolar (as indicated by the first index) deformability of the stars.

Love numbers have been also referred to as *apsidal motion constants* in the white-dwarf literature. See Sterne 1939.

For a white dwarf a radius R_s, the quadrupolar Love number k_2 can be calculated by solving the Clairaut-Radau equation

$$r\frac{d\eta_2}{dr} + \eta_2(r)(\eta_2(r)-1) + \frac{8\pi r^3\rho(r)}{m(r)}(\eta_2(r)+1) = 6 \tag{2.43}$$

with the boundary condition $\eta_2(0) = 0$, as

$$k_2 = \frac{3-\eta_2(R_s)}{2(2+\eta_2(R_s))}\,. \tag{2.44}$$

Here $\rho(r)$ and $m(r)$ relate to the unperturbed mass density at radius r and the mass contained in the sphere of radius r, as obtained from the hydrostatic equilibrium equations (2.4) and (2.5).

The quadrupolar Love number k_2 measures the degree to which mass is concentrated toward the center of the star. It tends to $k_2 = 0$ as more mass accumulates in the central core and is highest for an incompressible star with $\rho(r) = \rho_s$. In this latter case, Eq. (2.43) reduces to

$$r\frac{d\eta_2}{dr} + \eta_2(r)^2 + 5\eta_2(r) = 0\,. \tag{2.45}$$

The solution is simply $\eta_2(r) = 0$, leading to $k_2 = \frac{3}{4}$. For a polytropic equation of state $P = K\rho^\gamma$, k_2 is found to be independent of the white dwarf mass $m_s = m(R_s)$ and radius R_s (this is no longer true for more realistic equations of state). In particular, for ultrarelativistic electrons with $\gamma = \frac{4}{3}$, the Love number is much smaller than for an incompressible star and is approximately given by $k_2 \approx 0.014$.

Love numbers for polytropic equations of state were tabulated by Brooker and Olle 1955. For more realistic equations of state, see Perot and Chamel 2022.

3
Neutron stars

Contents

3.1 Neutron stars: predictions and discoveries

Speculation about stars even denser than white dwarfs

As far back as 1926, Ralph Fowler speculated on the possibility that matter even denser than white dwarfs might exist in nature, by

reasoning on the size of electrons and atomic nuclei[1]: "The 'volumes' of these are perhaps 10^{-14} of the volume of the corresponding atoms, so that densities up to 10^{14} times that of terrestrial materials may not be impossible". Was it possible to crush atomic nuclei against each other? Or could the nuclei resist compression to prevent the implosion of the most massive stars?

[1] R. H. Fowler. On dense matter. *Mon. Not. R. Astron. Soc.*, 87: 114–122, December 1926. DOI: 10.1093/mnras/87.2.114. URL https://doi.org/10.1093/mnras/87.2.114

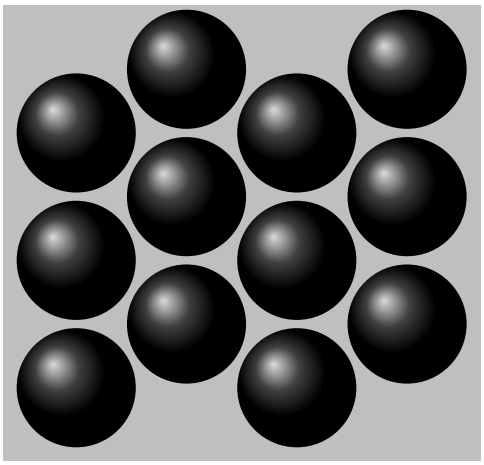

Figure 3.1: Schematic picture of matter at nuclear density $\sim 10^{14}$ g cm^{-3} in which nuclei are touching each other and coexist with a gas of free electrons.

Between February and March 1931 in Copenhagen, Landau speculated with Danish physicist Niels Bohr (one of the founding fathers of quantum mechanics and winner of the Nobel Prize in 1922) and Belgian physicist Léon Rosenfeld on the possible existence of stars even denser than white dwarfs, in which matter would be so compressed that atomic nuclei would fuse to form a single gigantic nucleus. Landau would not publish the results of these discussions until a year later, in February 1932, at the same time as Chadwick announced his discovery of the neutron. This coincidence of dates would later lead Rosenfeld to claim that Landau had envisaged stars composed mainly of neutrons[2].

In reality, the concept of *neutron stars* was first proposed by Swiss physicist Fritz Zwicky and German astronomer Wilhelm Baade in December 1933 at a meeting of the American Physical Society at Stanford University. Zwicky was a truculent character with a talent for coming up with the most extravagant ideas. He also had a reputation for having a terrible temper. He didn't hesitate to treat his colleagues with the utmost contempt. Very few were prepared to take this eccentric physicist seriously. Baade, on the other hand, was a renowned astronomer. At the time, Zwicky and Baade were working on *supernovae* (a term they had coined in 1931), very distant stars that suddenly became as bright as all the stars in the Galaxy combined. In the brief summary of their paper published in 1934, they concluded

[2] Dmitrii G. Yakovlev, Pawel Haensel, Gordon Baym, and Christopher Pethick. Lev Landau and the concept of neutron stars. *Physics Uspekhi*, 56(3):289-295, March 2013. DOI: 10.3367/UFNe.0183.201303f.0307. URL https://doi.org/10.3367/UFNe.0183.201303f.0307

with the phrase that would become famous a few decades later[3]: "We advance the view that supernovae represent transitions between ordinary stars and neutron stars, which in their final stages consist of extremely close packed neutrons". It was undoubtedly Baade who saw fit to add "with all reserve" as a preamble. At the time, astrophysicists believed that stars ended their existence in one of two ways: either they disappeared peacefully as white dwarfs, or they disintegrated completely in very violent explosions.

[3] W. Baade and F. Zwicky. Cosmic Rays from Super-novae. *Proceedings of the National Academy of Science*, 20(5):259–263, May 1934. DOI: 10.1073/pnas.20.5.259. URL https://doi.org/10.1073/pnas.20.5.259

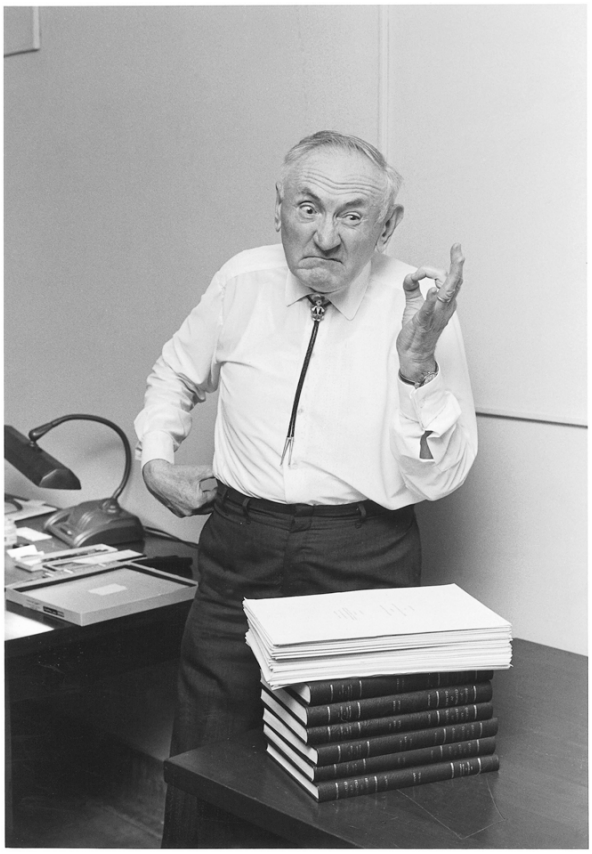

Figure 3.2: Fritz Zwicky

In 1937, Landau suggested that stars could draw their energy from the accretion of matter onto a neutron core. This possibility was also raised independently by physicist George Gamow. Nevertheless, he remained convinced that thermonuclear reactions provided the main source of energy for stars. A decade earlier, he had shown that quantum mechanics could allow particles to escape from a nucleus. This tunnel effect explained the emission of alpha particles (helium nuclei) by certain elements such as uranium. Gamow understood that nuclei in the hot cores of stars could fuse by the same tunnel effect, releasing phenomenal amounts of energy. However, the details of these nuclear processes were not elucidated until 1938 by the

physicist Hans Bethe. That same year, at the University of California, Berkeley, American physicist Robert Oppenheimer (best known for his involvement in the Manhattan Project) and his post-doc Robert Serber published a critical commentary on Landau's theory. Landau had estimated the minimum mass that a neutron core must have to be stable inside a star. But he had neglected nuclear forces. Oppenheimer and Serber showed that Landau had grossly underestimated the mass of the neutron core[4]. What is more, this neutron core would be surrounded by a region of degenerate matter, as in a white dwarf. If a star like the Sun had such a neutron core, it would consist almost entirely of degenerate matter. However, Eddington's model of stars as balls of perfect gas explained astronomical observations very well. Landau's theory therefore failed to resolve the question of the origin of stellar energy, at least in the case of low-mass stars like the Sun. But Oppenheimer and Serber were unaware that Landau's paper was a desperate attempt to escape the Stalinist purges. Despite Niels Bohr's support, he was arrested by the political police on April 28, 1938. Unjustly accused of spying for Nazi Germany, he was thrown into prison. He was released only a year later, thanks to the intervention of Piotr Kapitza (winner of the 1978 Nobel Prize in Physics for his work on superfluidity) with Stalin and Molotov.

[4] J. R. Oppenheimer and Robert Serber. On the Stability of Stellar Neutron Cores. *Physical Review*, 54(7):540–540, October 1938. DOI: 10.1103/PhysRev.54.540. URL https://doi.org/10.1103/PhysRev.54.540

Figure 3.3: Robert Oppenheimer (right) with Robert Serber (left) of the University of California's radiation laboratory at Berkeley, Calif., April 23, 1946. (AP Photo).

Oppenheimer's and Serber's calculations ruled out the presence of a neutron core in ordinary stars, but could there be neutron stars as

such, as Zwicky proposed? In August 1938, the latter sent a note to the Astrophysical Journal, in which he estimated the maximum mass of a neutron star at around 11 times the mass of the Sun[5]. Zwicky relied on the solution to Einstein's equations that physicist Karl Schwarzschild had found between 1915 and 1916 in the simplest case of an incompressible spherical star. In September, Bethe suggested that a massive star that had consumed its nuclear fuel would collapse in on itself until a neutron core was formed, its cohesion being ensured by neutron degeneracy pressure (Bethe's paper was not published until March of the following year, however). In November of the same year, Gamow argued that a star could generate a neutron core if its mass exceeded the Chandrasekhar mass limit (around one and a half times the mass of the Sun). He drew on Sterne's work published in 1933, which showed that, if matter was crushed sufficiently, electrons would eventually be captured by the nuclei and transformed into neutrons. Chandrasekhar evoked the same scenario at a conference in Paris in July 1939. For his part, Oppenheimer asked his student George Volkoff to calculate the maximum mass of a neutron core. Such an object is so compact that its modeling requires the application of Einstein's theory of general relativity. Guided by Richard Tolman, one of Caltech's leading experts in general relativity and cosmology, Volkoff obtained the differential equations describing a spherical star (according to Gordon Baym, these equations had been deduced independently by Chandrasekhar and John von Neumann as early as 1934). Volkoff numerically solved these equations by treating the interior of the neutron core as a degenerate quantum gas. At the time, nuclear forces were still very poorly understood. Oppenheimer and Volkoff decided to ignore them. The maximum mass of a stable neutron core they obtained turned out to be about half Chandrasekhar's mass. This work[6], published in February 1939, implied that a massive star at the end of its life would not form a stable neutron core as Bethe had assumed, but would inevitably collapse in on itself. In other words, Zwicky's *neutron stars* became purely academic objects. At the same time, Tolman published a paper in which he presented a series of analytical solutions to Einstein's equations, which led to a better understanding of the origin of the mass limit. In their article, Oppenheimer and Volkoff cited Landau's papers, but made no mention of those by Zwicky. Zwicky worked at Caltech as did Tolman, but Oppenheimer didn't see fit to meet him (Zwicky had spoken with Tolman a few months earlier, as evidenced by the note he sent to the Astrophysical Journal). Three months later, Zwicky in turn submitted an article on neutron stars to Physical Review[7] without any reference to Oppenheimer. In the first part of his paper, Zwicky discussed the maximum mass of a neutron

[5] F. Zwicky. On Collapsed Neutron Stars. *Astrophys. J.*, 88:522–525, November 1938. DOI: 10.1086/144003. URL https://doi.org/10.1086/144003

[6] J. R. Oppenheimer and G. M. Volkoff. On Massive Neutron Cores. *Physical Review*, 55(4):374–381, February 1939. DOI: 10.1103/PhysRev.55.374. URL https://doi.org/10.1103/PhysRev.55.374

[7]

star, but only in the idealized case of an incompressible star (whose structure had already been calculated by Schwarzschild between 1915 and 1916). In the second part, Zwicky dealt with the astrophysical consequences of neutron stars, notably the redshift of light emitted at the star's surface due to its intense gravitational field.

Equation of state of dense matter

During the Second World War, many leading physicists led by Oppenheimer took part in the Manhattan Project to develop the atomic bomb. The spectacular progress made in nuclear physics led to significant advances in the study of stellar collapse. In 1946-1947, the Dutch physicist Gale Bruno van Albada undertook the first detailed study of the composition of matter compressed to extremely high densities. In particular, he showed that nuclei become increasingly rich in neutrons as the compression ratio of matter increases. He also established that this neutronization of matter leads to the appearance of a neutron gas when the density reaches around 5×10^{11} g/cm^3. In the late 1950s, physicist John Archibald Wheeler of Princeton University in the USA introduced the concept of "perfectly catalyzed cold matter in the final stage of thermonuclear evolution". His aim was to understand the final state of a star that had burnt itself out and cooled down to a state of thermodynamic equilibrium at absolute zero temperature. Wheeler asked his student B. Kent Harrison to calculate the pressure of catalyzed cold matter as a function of density. Up to around 10^4g/cm^3, this matter is iron. Above that, the material is so compressed that electrons are stripped from the atoms. For densities above 10^6 g/cm^3, electrons reach speeds close to the speed of light. The electrons are sufficiently tightly packed onto the nuclei to alter their composition. A neutron gas appears at around 3×10^{11} g/cm^3. When the density reaches around 5×10^{12} g/cm^3, the pressure is mainly provided by the neutron gas. For even higher densities, Wheeler and Harrison assumed that matter consists of a mixture of neutrons, protons and electrons with no interactions.

Wheeler asked a Japanese student, Masami Wakano, to calculate the structure of a star composed of cold catalyzed matter using Einstein's equations. They were thus able to describe stars as different as an iron planet, a white dwarf and a neutron star within the same theoretical framework. They proved that there is no stable star with a central density intermediate between that of a white dwarf and a neutron star. Their calculations also demonstrated that mass density never becomes infinite at the center of a white dwarf star, contrary to the results obtained by Chandrasekhar, who had not taken neutronization of matter into account (the French astrophysicist Evry

Schatzman had already reached the same conclusion two years earlier). The maximum mass of a neutron star they obtained was slightly lower than Oppenheimer's, due to the presence of protons and electrons in the star's core. Wheeler presented the results of his work at the eleventh Solvay Physics Conference at the Université Libre de Bruxelles in June 1958[8]. Oppenheimer was also present. The question of the fate of massive stars was hotly debated. Unlike Oppenheimer, Wheeler was convinced that a massive star could never collapse on itself into a point of infinite density. Even in the absence of mass ejection, Wheeler believed that the compression of matter would generate radiation which, as it escaped from the star, would reduce its mass below the mass limit (due to the equivalence between mass and energy in Einstein's famous equation $E = mc^2$).

[8] B. K. Harrison, M. Wakano, and J. A. Wheeler. Matter-energy at high density: end point of thermonuclear evolution. In *Onzième Conseil de Physique Solvay, Stoops, Brussels*, page 124, 1958

A decisive step was taken in 1959 by Canadian astrophysicist Alastair G. W. Cameron[9], who emphasized the importance of nuclear forces in calculating the structure of a neutron star. In particular, he showed that the forces between neutrons squashed against each other are so repulsive that they increase the maximum mass of a neutron star to around twice the mass of the Sun (a value very close to current models), i.e. beyond the Chandrasekhar mass. Cameron also pointed out that the core of a neutron star could contain various types of particles, including hyperons. A neutron star could therefore be formed by the collapse of a sufficiently massive ordinary star (with a mass greater than Chandrasekhar's but less than twice the mass of the Sun), as Baade and Zwicky had predicted. This scenario was confirmed in the following years by computer simulations of a stellar implosion. These simulations, carried out in particular by American physicists and independently by Soviet physicists, also showed that the most massive stars inexorably contracted until they formed a singularity, as Oppenheimer had predicted. Wheeler was finally convinced, and popularized the term *black hole* to designate these new objects (see Kip Thorne's fascinating account[10]).

[9] A. G. Cameron. Neutron Star Models. *Astrophys. J.*, 130:884, November 1959. DOI: 10.1086/146780. URL https://doi.org/10.1086/146780

[10] Kip S. Thorne. *Black holes and time warps: Einstein's outrageous legacy*. 1994

Discovery of mysterious X-ray sources

In the late 1940s, a group of American scientists led by Herbert Friedman discovered that the Sun is a source of X-rays, using scientific instruments installed on V-2 rockets built by the Nazis and recovered by the US army at the end of the Second World War. These experiments also showed that most of these X-rays are absorbed by the atmosphere. Towards the end of the 1950s, a research program was launched in the United States under the impetus of Riccardo Giacconi to observe the sky in X-rays. Rockets equipped with increasingly sophisticated detectors were sent into space in the 1960s. The first

extra-solar X-ray source, named Sco X-1, was discovered in June 1962 in the constellation Scorpius. Several other sources were soon identified. Unlike the Sun, these sources appeared very bright in the X-ray range, but very faint in the visible spectrum. In 1963, Japanese astrophysicists Satio Hayakawa and Masaru Matsuoka envisioned a system of two stars orbiting each other. One of the stars was supposed to be a supergiant star so luminous that it would eject matter in the form of a particle wind. As it passed through this wind, the companion star would produce a shock wave that would give rise to the X-rays observed. Unfortunately, the X-ray sources did not appear to be associated with any supergiant stars. At a symposium of the International Astronomical Union in 1966, astrophysicist Geoffrey Burbidge suggested that the wind might originate not from a supergiant star, but from a neutron star. In 1967, Soviet astrophysicist Iosif Shklovsky developed a model in which X-ray sources are stellar pairs formed by an ordinary star whose matter is literally sucked into a neutron star. Soviet physicists Yakov Zeldovich and Igor Novikov had already shown in 1965 that the accretion of matter onto a neutron star would give rise to X-ray emission. Unfortunately, no X-ray variability was detected that could have betrayed the presence of a neutron star. Nevertheless, some X-ray sources were discovered in supernova remnants. If Baade and Zwicky's scenario was correct, these sources were prime targets for neutron star detection. In particular, the detection of X-ray emission in the Crab Nebula in April 1963 gave rise to a great wave of hope.

See Wallace and Giacconi 1985 for a detailed account of X-ray astronomy.

The iconic Crab Nebula

The Crab Nebula was discovered in 1731 by a British amateur astronomer named John Bevis, and independently by the French astronomer Charles Messier in 1758. It became the first item in his famous catalog of diffuse objects published in 1771. The nebula's current name was introduced in 1848 by William Parsons, third Earl of Rosse and a remarkable astronomer. Owning the largest telescopes of his time, he thought he saw "singularly arranged filaments" in the nebula, which reminded him of a crab. In March 1921, astronomer Carl Otto Lampland at the Lowell Observatory observed changes in the Crab Nebula by comparing different images taken over a period of eight years. Shortly afterwards, astronomer John Charles Duncan of the Mount Wilson Observatory showed that the nebula had been expanding for several hundred years. A few months later, Knut Lundmark pointed out that on July 4, 1054, Chinese astronomers had noted the appearance of a "new star" or *nova* in the Taurus constellation at a position close to that occupied by the Crab nebula.

See Mitton 1979 for a detailed account of the discoveries of the Crab Nebula.

Lundmark relied in particular on the work of French astronomer Jean-Baptiste Biot and his sinologist son Édouard Biot. According to Chinese astronomers, this "guest star" remained visible in full daylight for almost a month, and only disappeared from the night sky after two years. Similar observations were reported by Japanese and Arab astronomers. Amerindian tribes living in the south-western part of today's United States a thousand years ago could also have tracked this event, as seems to be attested by the discovery of petroglyphs and cave paintings depicting a crescent Moon associated with what looks like a shiny object. On the morning of July 5, 1054, in the southwestern United States, the Moon occupied a position in the sky very close to that of the guest star. What is more, the crescent Moon is a symbol that was rarely used in Native American art. No trace of this astronomical phenomenon has been found in the contemporary writings of European astronomers. At the time, the latter were strongly influenced by Aristotelian philosophy, according to which the celestial world is unalterable, as opposed to the corruptible and changeable terrestrial world. As a result, European astronomers may well have lost interest in these star-appearing phenomena. In 1928, American astronomer Edwin Hubble suggested that the Crab Nebula might represent the remains of a stellar explosion. By measuring the rate of expansion of the nebula, he deduced that the explosion had taken place 900 years earlier, and linked this event to the "guest star" observed in 1054. This interpretation became widely accepted in the 1930s, particularly in the wake of Baade and Zwicky's work on supernovae.

In 1942, Baade and Rudolph Minkowski identified a star in the vicinity of the center of the Crab Nebula, which they believed to be the remnant of the supernova of 1054. This star was very different from ordinary stars. Its spectral analysis indicated that it must have been very hot and very compact, lending credence to the theory that it had imploded. However, astronomers were unable to explain the energy source behind the nebula's expansion. In particular, Baade showed that the radiation pressure of the central star was insufficient. What is more, the central mass of gas forming the nebula itself exhibited a mysterious continuous spectrum that seemed incompatible with radiation of thermal origin. This problem was exacerbated by the discovery of a radio source in 1948 by J.G. Bolton and G. J. Stanley. In 1953, Iosif Shklovsky put forward a revolutionary hypothesis. He suggested that the Crab Nebula's electromagnetic emission was due to synchrotron radiation generated by electrons spinning extremely rapidly around the lines of a very intense magnetic field. This interpretation was vividly confirmed a few months later by the discovery of the radiation's polarization. In 1964, astrophysicist

Figure 3.4: Image of the Crab nebula from the James Webb Space Telescope. Credit: NASA, ESA, CSA, STScI, T. Temim (Princeton University).

Lodewijk Woltjer and, independently of him, Soviet physicist Vitaly Ginzurg showed that a neutron star could possess a very intense magnetic field simply by conserving the magnetic flux during the collapse of the progenitor star.

At the same time, astrophysicists realized that if neutron stars were formed by the implosion of massive stars in supernovae, as Baade and Zwicky had proposed in 1933, they should have surface temperatures of several million degrees, and therefore shine mainly in the X-ray range. An X-ray source was detected in April 1963 in the direction of the Crab Nebula. Most astrophysicists were convinced that it was a neutron star associated with the supernova of 1054. Shklosky and colleagues suggested observing the source during a lunar occultation to determine its size. If the X-ray source were indeed a neutron star, it would have to emanate from a very localized region of the nebula. As a result, the intensity of the radiation should drop to zero as the Moon passes in front of the nebula. An Aerobee rocket was launched on July 7, 1964 from White Sands Air Force Base in Arizona. Despite the success of the space mission, the results were disappointing. Measurements indicated that at least 90% of the X-ray emission came from the nebula itself. The remaining 10% could still be due to the presence of a neutron star. However, spectral analysis of the X-ray radiation carried out a few weeks later using a sound-

ing balloon seemed to invalidate this hypothesis. At the same time, radio observations were becoming increasingly precise. In 1965, Anthony Hewish and his Nigerian student Samuel Okoye discovered a flickering source and speculated that it might be "the remains of the original star that exploded". In 1966, John Wheeler mentioned in a journal article that a rapidly rotating neutron star could be powering the Crab Nebula. This idea was developed the following year by Franco Pacini, then a post-doctoral fellow at Cornell University. A few months later, radio astronomers at Cambridge discovered mysterious pulsating radio sources.

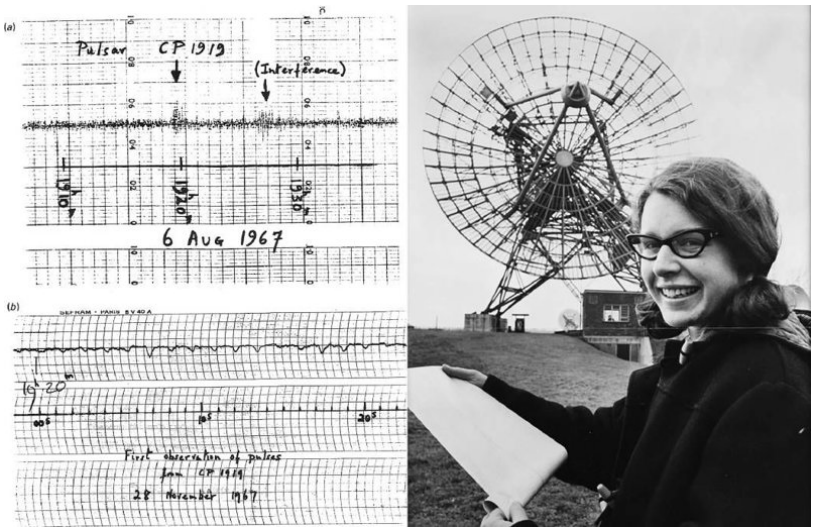

Figure 3.5: A photograph of Jocelyn Bell Burnell (born 1943) at the Mullard Radio Astronomy Observatory at Cambridge University, taken for the Daily Herald newspaper in 1968. Daily Herald Archive, SSPL, Getty Images.

Fortuitous discovery of pulsars

Neutron stars were finally discovered completely unexpectedly in the late 1960s. The story begins in 1965 at the Cavendish Laboratory in Cambridge, England. A young student named Jocelyn Bell, under the guidance of Anthony Hewish, began research into the study of radio wave scintillation. To this end, they built a radio telescope capable of making measurements on extremely short time scales. The telescope, comprising an array of 2048 antennas, was completed in July 1967. One month after commissioning, Jocelyn Bell detected a variable source. Subsequent observations revealed a signal of such extraordinary regularity that the source was given the acronym LGM for "Little Green Men". Today, the source is known as PSR B1919+21. By the time the results were published in the prestigious journal Nature in February 1968, three other pulsating sources had been discovered, rendering obsolete the hypothesis of signals sent by an

extraterrestrial civilization. A Daily Telegraph journalist dubbed them *pulsars* (a neologism derived from the contraction of pulsating stars). A few months later, Thomas Gold theorized in a Nature article that pulsars are rapidly rotating neutron stars with very strong magnetic fields. In the same issue of Nature, Burbidge and Strittmatter pointed out that the periodic motion of the satellite Io around Jupiter was the source of radio waves, suggesting a similar phenomenon for pulsars. The hypothesis considered by Hewish and Bell was that of white dwarf vibrations. The question of the true nature of pulsars remained controversial until the end of 1968, when three crucial observations were made. In October, astronomers from the University of Sydney discovered a pulsar in the Vela constellation with a period of 89 milliseconds. Such rapid variation was hardly compatible with the white dwarf hypothesis. What's more, the pulsar was located in the remains of a supernova, suggesting an association with a neutron star. In November, a pulsar was detected by astronomers at the Green Bank Observatory in the famous Crab Nebula. With a period of just 33 milliseconds, this pulsar marked the end of white dwarf theories. A month later, the same astronomers noticed that the period of the Crab pulsar decreased very slightly over time. This observation contradicted both the neutron star vibration model and that of a pair of neutron stars. The only viable model was that of an isolated neutron star rotating around itself. Four decades after Baade and Zwicky's seminal paper, the reality of neutron stars was finally established. In 1974, Anthony Hewish was awarded the Nobel Prize in Physics. The same year, American radio astronomer Joseph Taylor and his student Russell Hulse discovered the first binary system to house a pulsar, whose meticulous observation provided indirect evidence for the existence of gravitational waves. They were awarded the Nobel Prize in physics in 1993. To date, more than 3500 pulsars have been identified, representing a tiny fraction of the neutron star population in our Galaxy . Today, neutron stars are actively tracked and scrutinized at all wavelengths of electromagnetic radiation, from radio waves to gamma rays, by telescopes on the ground and in space. Riccardo Giacconi's pioneering work in X-ray observation was awarded the Nobel Prize in Physics in 2002.

3.2 *Hulse-Taylor pulsar and gravitational waves*

The pulsar PSR B1913+16 was first detected in July 1974 by Joseph Taylor and Russel Hulse. The period of 59 ms was found to be changing by up to $\Delta P_{\rm orb} = 80\mu$s from day to day. This was a really huge variation compared to $\sim 10\mu$s/year for pulsars known at that time, and was soon interpreted as being due to the Doppler shift from the

orbital motion of the pulsar around some unseen companion. The relative change of the period is then given by $\frac{\Delta P_{\rm orb}}{P_{\rm orb}} = \frac{v_p}{c}$, where v_p is the velocity of the pulsar along the line of sight, which in turn can be expressed as

$$\frac{v_p}{c} = \frac{\omega x_p}{\sqrt{1-e^2}} \left[\cos(\psi+\Phi) + e\cos\psi\right] , \tag{3.1}$$

where

$$x_p = \frac{a_p}{c}\sin i , \tag{3.2}$$

a_p is the semi major axis of the pulsar's orbit, i is the inclination of the orbital plane to the line of sight, $\omega = \frac{2\pi}{P_{\rm orb}}$, ψ is the periastron phase, Φ is the orbital phase, and e is the eccentricity. Fitting the observed velocity v_p as a function of the orbital phase Φ yields $P_{\rm orb} \approx$7h45min, $e \approx 0.617$, $x_p \approx 2.34$ s, as well as ψ and the time of the periastron passage from which the advance of the perisatron can be inferred, $\dot\psi \approx 4.23^\circ$/year. This is to be compared with 43"/century measured for Mercury! The periastron advance is given by Eq. (1.42), which can be equivalently written using Kepler's law (1.15) as

$$\dot\psi = \frac{3}{c^2}\frac{a^2}{1-e^2}\left(\frac{2\pi}{P_{\rm orb}}\right)^3 . \tag{3.3}$$

Here a is the semimajor axis of the orbit of the reduced mass. The semimajor axis of the pulsar's orbit is given by

$$a_p = a\frac{m_c}{m_p+m_c} , \tag{3.4}$$

where m_p and m_c are the masses of the pulsar and of the companion respectively. From measurements of $P_{\rm orb}$, e, and $\dot\psi$, the semimajor axis can be determined $a \approx 2.2\times10^6$ km $\approx 3R_\odot$. The total mass can be inferred from Kepler's law:

$$m = m_p + m_c = \frac{a^3}{G}\left(\frac{2\pi}{P_{\rm orb}}\right)^2 \approx 2.83 M_\odot . \tag{3.5}$$

The small orbit, the absence of eclipse, and the huge advance of the periastron indicate that the companion must be a compact star and both objects can be treated as point like. The relative shift of the pulse arrival times due to the quadratic Doppler effect and gravitational redshift in the field of the companion allows to measure the so called Einstein parameter

$$\gamma = e\left(\frac{P_{\rm orb}}{2\pi}\right)^{1/3}\frac{G^{2/3}}{c^2}\frac{m_c(m+m_c)}{m^{4/3}} \approx 4.29\times10^{-3}\ {\rm s} , \tag{3.6}$$

from which the individual masses of the pulsar and the companion can be estimated: $m_p \approx 1.44 M_\odot$ and $m_c \approx 1.39 M_\odot$. The companion

is most likely a neutron star. The inclination can be inferred from x_p using Eq. (3.4) and is $i \approx 47°$. The orbital parameters are now completely determined.

The orbital decay of the orbital period corrected for galactic acceleration $\dot{P}_{\rm orb} \approx 2.4056 \times 10^{-12}$s/s can now be compared with predictions from general relativity using Eq. (1.34):

$$\dot{P}_{\rm orb} = -(2\pi)^{8/3}\frac{96}{5}\left(\frac{G\mathcal{M}}{P_{\rm orb}c^3}\right)^{5/3} f(e)\,. \tag{3.7}$$

The excellent agreement (less than 0.1%) was an indirect proof of the existence of gravitational waves. For their discovery, Hulse and Taylor were awarded the Nobel Prize in 1993. The time to merger (1.40) is about $\tau \approx 306$ Myr. The effects of eccentricity are quite significant and reduce τ by a factor of ~ 5 compared to circular orbits.

The gravitational luminosity (1.30) represents about 2% of the (electromagnetic) luminosity of the Sun. The pulsar is located at a distance of about 5 kpc. The flux we receive is found to be very small $F \approx 2.6 \times 10^{-14}$ erg/cm^2/s. Because of the eccentricity of the orbit, gravitational waves are emitted are multiple harmonics. The peak occurs for $n_{\rm peak} \sim 7$ at a frequency $f_{\rm peak} \approx 115$ Hz. This lies within the frequency range of ground-based interferometers but the gravitational wave amplitude is too small to be detectable.

3.3 *Formation and evolution of neutron stars*

Evolution of massive stars and core-collapse supernova explosions

In stars with a mass $\gtrsim 8 - 10M_\odot$ (on the main sequence), fusion reactions proceed beyond hydrogen burning and yield heavier and heavier elements such as neon, magnesium, silicon up to iron peak elements (mainly ^{54}Fe, ^{56}Fe, and ^{56}Ni) in shorter and shorter times, see Table 3.1. The interior of the star thus exhibits an onion-like layered structure, as illustrated in Fig. 3.6.

	T (K)	ρ (g/cm^3)	duration
H	3.5×10^7	5.8	11 Myr
He	1.8×10^8	1.4×10^3	2 Myr
C	8.3×10^8	2.4×10^5	2 kyr
Ne	1.6×10^9	7.2×10^6	0.7 yr
O	1.9×10^9	6.7×10^6	2.6 yr
Si	3.3×10^9	4.3×10^7	18 days

Table 3.1: Core temperature T, core density ρ and duration of various burning stages in the a star of $15M_\odot$. From Woosley et al. 2002.

At this point, nucleosynthesis processes in the core stop since these nuclei are the most stable. Their relative abundances depend on temperature, density, and electron fraction. The inert core becomes

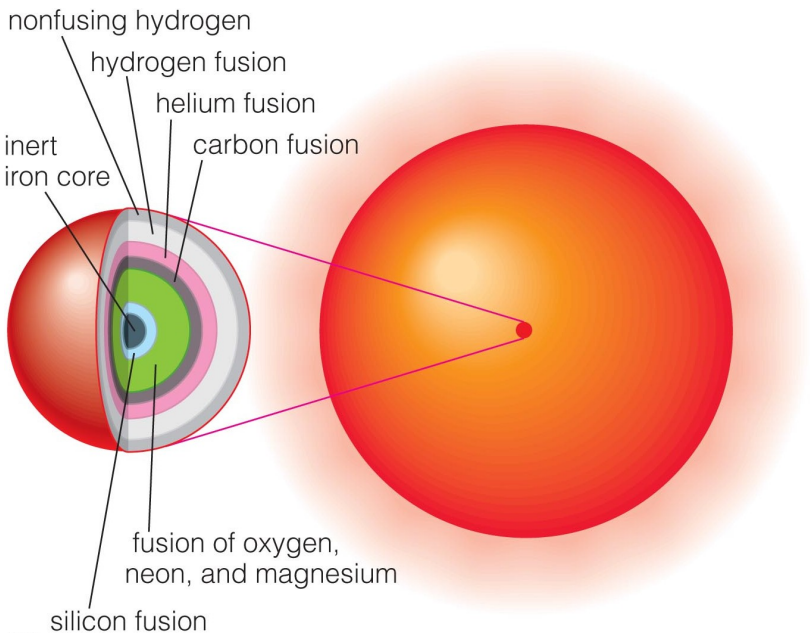

Figure 3.6: Schematic structure of a massive star at the end of the last core burning stage.

degenerate and sustained by the electron degeneracy pressure as white dwarfs. But the reactions proceed in the outer layers. Silicon fusion produces new iron nuclei, which fall into the core and increase its mass. When the mass exceeds the Chandrasekhar limit, the core collapses. The collapse is accelerated by electron captures by nuclei (2.30) (the conversion of protons into neutrons lowers the maximum mass, as can be seen from Eq.(2.26)) and photodisintegration

$$^{56}\mathrm{Fe} + \gamma \rightarrow 13\,^{4}\mathrm{He} + 4n\,. \tag{3.8}$$

In about 1 second, the core shrinks from a radius $\sim R_\oplus$ to $\sim 50km$. When the density of the core reaches $\sim 10^{12}$ g cm^{-3}, neutrinos are "trapped" (their diffusion time exceeding the collapse time). The collapse stops when matter becomes as dense as atomic nuclei (density of the order of 10^{14} g cm^3) due to the strongly repulsive nuclear interactions. The core bounces violently, creating a shock wave. This shock waves loses most of its energy from the infalling outer layers. The revival of the shock is not completely understood but neutrino energy deposition and magnetohydrodynamical instabilities are thought to play important roles. If the shock wave remains powerful enough, the envelope is expelled releasing a colossal amount of energy $\sim 10^{53}$ erg in a supernova explosion: $\sim 99\%$ in the form of neutrinos, $\sim 1\%$ in the kinetic energy of the ejecta. Even though only $\lesssim 0.01\%$ of the energy is radiated in photons, core-collapse supernova explosions are as luminous as billions of stars. At the same time, the

explosion seeds the interstellar medium with heavy elements.

Figure 3.7: Observation of the supernova SN1987A ten days after the explosion (left panel) compared to the same image of the sky before the explosion (right panel). Credit: Anglo-Australian Observatory.

Such an event designated SN1987A at a distance of about 51 kpc was observed in the Large Magellanic Cloud on February 24, 1987, as shown in Fig. 3.7. About 24 neutrinos were also received on Earth within ten seconds and confirmed the above scenario of gravitational core-collapse supernova explosions, in particular the neutronisation of matter and the fact that most energy is carried away by neutrinos. The type of remnant depends on the amount of ejected material falling back and on the mass of the collapsing core, which in turn depends on the progenitor mass and mass loss. Stars with lower metallicity than the Sun have weaker winds and therefore retain most of their mass. The compact remnant of SN1987A is expected to be a neutron star. It has not yet been directly detected, but recent observations using the James Webb Space Telescope suggest the presence of a neutron star[11].

Stars whose mass on the main sequence lies within $\sim 8-10M_\odot$ may produce neutron stars due to electron captures by ^{24}Mg and ^{20}Ne in so called electron-capture supernova. Those neutron stars are expected to have a mass close to the Chandrasekhar limit, $\sim 1.4M_\odot$ for an O-Ne core. The Crab pulsar is thought to have been formed in this way. Stars with solar metallicity and a mass $\lesssim 15M_\odot$ are predicted to end up in neutron stars. The fate of more massive stars depends on other factors.

[11] C. Fransson et al. Emission lines due to ionizing radiation from a compact object in the remnant of supernova 1987a. *Science*, 383(6685):898–903, 2024. DOI: 10.1126/science.adj5796. URL https://www.science.org/doi/abs/10.1126/science.adj5796

Cooling of neutron stars

Initially very hot with temperatures of order $\sim 10^{11} - 10^{12}$ K, a neutron star becomes transparent to neutrinos copiously produced in its interior and thus rapidly cools down. After a few days, the temperature drops to $\sim 10^9$ K and the outer layers start to crystallize from the interior to the surface. At this stage, the highly degenerate core is much colder than the crust. After several decades, the star becomes isothermal with a temperature $\sim 10^8$ K except for a thin "heat-blanketing" envelope. The last cooling stage takes places after about 10^5 years when heat from the interior diffuses to the surface and is dissipated via electromagnetic radiation.

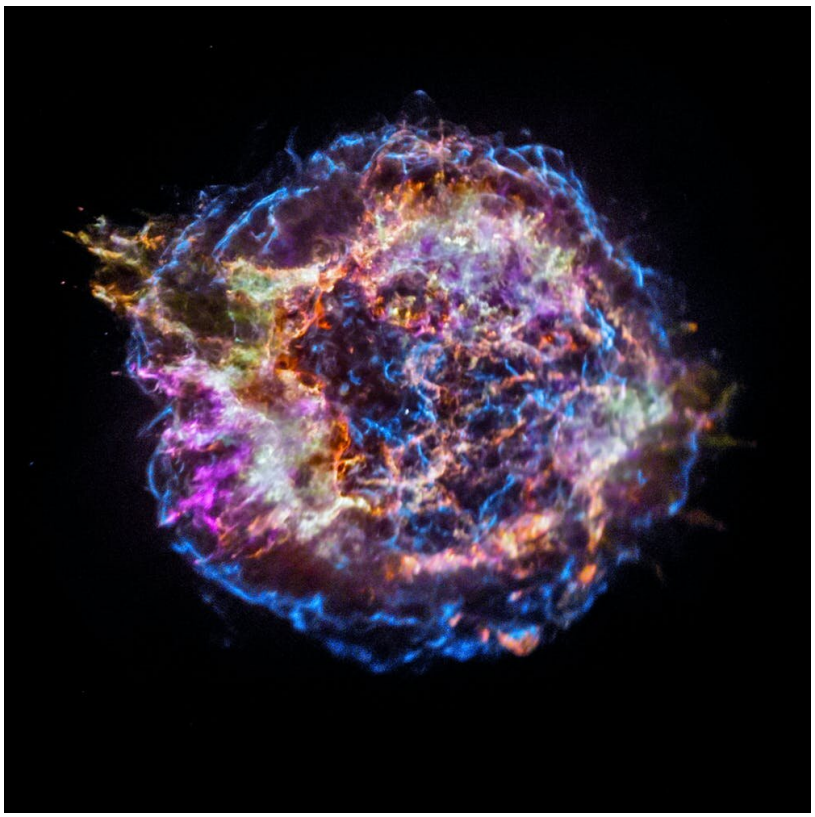

Figure 3.8: Image of the Cassiopeia A supernova remnant from NASA's Chandra X-ray observatory. The color scheme used in this image is the following: low-energy X-rays are red, medium-energy ones are green, and the highest-energy X-rays are colored blue. The neutron star is visible as a small white spot a the center. Credit: NASA/CXC/SAO.

Most observed neutron stars are old and "cold" (recalling that typical nuclear energies are measured in MeV corresponding to temperatures of order 10^{10} K). The youngest known neutron star in the Cassiopeia A supernova remnant is about 360 years old, see Fig. 3.8.

3.4 *Structure of a neutron star*

Internal constitution

Neutron stars are expected to be surrounded by a very thin atmosphere consisting of a plasma of electrons and light elements (mainly hydrogen and helium though heavier elements like carbon may also be present). Its properties such as the effective temperature, the composition, and the magnetic field configuration, can be inferred by analyzing the thermal X-ray emission from neutron stars.

The outermost region of a nonaccreting neutron star is expected to be made of iron ^{56}Fe (the end-product of stellar nucleosynthesis), possibly with a small admixture of other elements as a result of the accretion of matter or the fallback of material from the envelope ejected during the supernova explosion. This prediction is supported by the identification of broad Fe K emission lines thought to originate from the accretion disk around neutron stars in low-mass X-ray binaries. The properties of compressed iron can be probed in terrestrial laboratories up to pressures of order 10^{14} dyn cm^{-2} with nuclear explosions and laser-driven shock-wave experiments. Under these conditions, iron has an hexagonal close-packed structure. Transitions to a face-centered cubic lattice and a body-centered cubic lattice are expected at pressures of about 6×10^{13} dyn cm^{-2} and 4×10^{14} dyn cm^{-2} respectively for temperatures below $\sim 10^4 - 10^5$ K. Although such pressures are tremendous according to terrestrial standards, they still remain negligibly small compared to those prevailing in a neutron star. In particular, the highest density of iron that has been experimentally attained is only about three times the density at the surface of a neutron star, and 14 orders of magnitude lower than the density at the center. This corresponds to a depth of about 0.1 mm for a star with a mass of $1.4\mathcal{M}_\odot$ and a radius of 12 km. Deeper in the star, recourse must therefore be made to theoretical models.

With average densities ranging from a few grams per cubic centimeter at their surface to about 10^{15} g cm^{-3} in their core, the interior of a neutron star is expected to exhibit very different phases of matter. Below the surface in the so-called *outer crust*, at densities above $\rho \sim 10^4$ g cm^{-3}, matter consists of a body-centered cubic crystal of fully ionized atoms coexisting with a degenerate electron gas. With increasing density, nuclei become progressively more neutron rich as a result of electron capture. At a density of about $\sim 4 \times 10^{11}$ g cm^{-3}, neutrons begin to drip out of the nuclei, marking the transition to the *inner crust*, which is composed of an inhomogeneous assembly of neutron-proton clusters immersed in a neutron ocean and neutralized

by the degenerate electron gas.

When the density reaches about $\sim 10^{14}$ g cm^{-3} (about half the density found in heavy atomic nuclei), the crust dissolves into a homogeneous mixture of neutrons with a small admixture of protons, neutralized by electrons and, at slightly higher densities, muons, thus forming the so-called *outer core*. The *inner core* of massive neutron stars may contain other particles like hyperons, or even deconfined quarks.

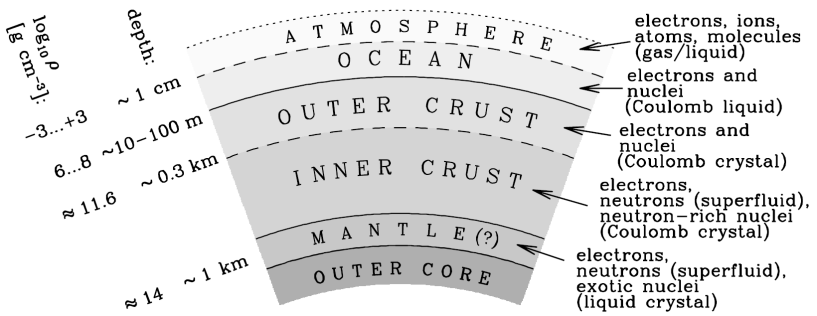

Figure 3.9: Schematic structure of the interior of a neutron star with an internal temperature $\sim 10^8$ K. From Haensel et al. 2007.

Tolman-Oppenheimer-Volkoff equations

As discussed previously, observed neutron stars are old and cold. In the cold catalyzed matter hypothesis, the neutron star is supposed to have reached is lowest possible energy state. The neutron star is necessarily static without any viscous or elastic stress. The interior of the star can therefore be treated as a perfect fluid. The stress-energy tensor is given by

$$T^{\mu\nu} = \left(\rho + \frac{P}{c^2}\right) u^\mu u^\nu + P g^{\mu\nu}\,, \tag{3.9}$$

where ρ is the mass-energy density, P is the pressure, $u^\mu = \dfrac{dx^\mu}{d\tau}$ denotes the fluid four-velocity normalized as $g_{\mu\nu}u^\mu u^\nu = -c^2$ using the metric signature $(-+++)$, τ being the proper time. The global structure of the neutron star can be determined from Einstein's equations

$$\mathscr{R}^{\mu\nu} - \frac{1}{2}\mathscr{R} g^{\mu\nu} + \Lambda g^{\mu\nu} = \frac{8\pi G}{c^4} T^{\mu\nu}\,, \tag{3.10}$$

where $\mathscr{R}^{\mu\nu}$ is the Ricci tensor and $\mathscr{R}$ is the Ricci scalar. The cosmological constant term with Λ is negligible at stellar scale and can therefore be ignored.

The most general metric of a spherically symmetric static spacetime can be written as

$$ds^2 = -c^2 d\tau^2 = -e^{2\Phi(r)} c^2 dt^2 + e^{2\lambda(r)} dr^2 + r^2(d\theta^2 + \sin^2\theta d\phi^2)\,. \tag{3.11}$$

Note that the proper radial distance from the center of the star to the radial coordinate r is not simply given by r. Fixing t, θ, and ϕ and integrating the spacetime interval ds from 0 to r leads to

$$\int_0^r dr' e^{\lambda(r')} \neq r\,. \tag{3.12}$$

The coordinate r can be interpreted as the circumferential radius since the perimeter $\mathscr{P}$ obtained by fixing t, r, $\theta = \frac{\pi}{2}$ and integrating the spacetime interval ds over ϕ is given by

$$\mathscr{P} = R\int_0^{2\pi} d\phi = 2\pi R\,. \tag{3.13}$$

Outside the star, $T^{\mu\nu} = 0$ and the metric reduces to that of Schwarzschild:

$$e^{2\Phi(r)} = 1 - \frac{2Gm_s}{rc^2}\,, \tag{3.14}$$

$$e^{2\lambda(r)} = \left(1 - \frac{2Gm_s}{rc^2}\right)^{-1}\,, \tag{3.15}$$

where m_s is the mass of the star. Imagine a source emitting dN periodic signals from the stellar surface during $d\tau$ with a frequency

$$f_s = \frac{dN}{d\tau} = \frac{dN}{dt}e^{-\Phi(R_s)}\,. \tag{3.16}$$

A distance observer will detect signals with a frequency

$$f_\infty = \frac{dN}{dt}\,, \tag{3.17}$$

since $\Phi(r \to +\infty) = 0$ (the space time is asymptotically flat). Comparing Eqs. (3.16) and (3.4), the signal is thus found to be redshifted

$$f_\infty = f_s\sqrt{1 - \frac{2Gm_s}{R_s c^2}}\,. \tag{3.18}$$

The gravitational redshift is defined as

$$\boxed{z \equiv \frac{f_s - f_\infty}{f_\infty} = \left(1 - \frac{2Gm_s}{R_s c^2}\right)^{-1/2} - 1}\,. \tag{3.19}$$

Inside the star, we introduce the mass $m(r)$ such that

$$e^{2\lambda(r)} \equiv \left(1 - \frac{2Gm(r)}{rc^2}\right)^{-1}\,. \tag{3.20}$$

Einstein's equations can be recast into the Tolman-Oppenheimer-Volkoff (TOV) equations:

$$\boxed{\frac{dP}{dr} = -\frac{Gm\rho}{r^2}\left(1+\frac{P}{\rho c^2}\right)\left(1+\frac{4\pi r^3 P}{mc^2}\right)\left(1-\frac{2Gm}{rc^2}\right)^{-1}}, \tag{3.21}$$

$$\boxed{\frac{dm}{dr} = 4\pi r^2 \rho}, \tag{3.22}$$

$$\boxed{\frac{d\Phi}{dr} = -\frac{1}{\rho c^2}\frac{dP}{dr}\left(1+\frac{P}{\rho c^2}\right)^{-1}}. \tag{3.23}$$

The radius R_s of the star is defined by the condition $P(R_s) = 0$ to ensure continuity with the vacuum solution outside the star. The mass of the star is then given by $m_s = m(R_s)$. To solve these equations, the equation of state $P(\rho)$ of the matter constituting the star must be specified.

In practice, the pressure $P(r)$ and mass $m(r)$ are calculated for a given central density $\rho_c = \rho(0)$ by integrating Eqs. (3.21) and (3.22) from the center of the star up to the radial coordinate for which the pressure vanishes. The metric function $\Phi(r)$ is then determined by integrating Eq. (3.23) with the boundary condition

$$\Phi(R_s) = \frac{1}{2}\ln\left(1-\frac{2Gm_s}{R_s c^2}\right). \tag{3.24}$$

In the Newtonian limit $P \ll \rho c^2$, $Pr^3 \ll mc^2$, and $\frac{2Gm}{rc^2} \ll 1$, Eqs. (3.21) and (3.22) reduce to Eq. (2.4) and (2.5) respectively, whereas Eq. (3.23) becomes

$$\frac{1}{r^2}\frac{d}{dr}r^2\frac{d}{dr}c^2\Phi = 4\pi G\rho\,. \tag{3.25}$$

This is Poisson's equation for the gravitational potential $U(r) = -\Phi(r)c^2$.

Comparing Eqs. (3.21) and (2.4), it can be seen that general relativity increases the gravitational pull on matter: not only are the three factors in parentheses in the right-hand of side of Eq. (3.21) larger than 1, but the density ρ is also increased since in relativity it is defined not just by the mass density but through the energy density of matter $\mathcal{E}$ as $\rho = \frac{\mathcal{E}}{c^2}$. At first sight, the equation for the mass $m(r)$ appears to be deceptively unchanged. One has to remember that the proper volume element is generally defined as $dV = d^3r\sqrt{\tilde{g}}$, where $\tilde{g}$ is the determinant of the space metric. For the metric (3.11), the proper volume is found to be given by

$$dV = 4\pi r^2\left(1-\frac{2Gm}{rc^2}\right)^{-1/2}dr\,. \tag{3.26}$$

The mass of the star m_s defined through the integration of Eq. (3.22) by

$$m_s = \int_0^{R_s} dr\, 4\pi r^2 \rho(r)\,, \tag{3.27}$$

represents the *gravitational mass* of the star, and includes the binding energy of the gravitational field. It is lower than the *baryon mass* m_b defined as the total number of baryons in the star multiplied by their mass or equivalently

$$m_b = \int_0^{R_s} dr\, 4\pi r^2 \left(1 - \frac{2Gm}{rc^2}\right)^{-1/2} \rho_m(r) > m_s\,, \tag{3.28}$$

where $\rho_m(r)$ is the mass density.

Finally, let us remark that the TOV equation (3.21) can be derived from a variational principle by minimizing the gravitational mass (3.27) for any given baryon mass (3.28) (see Harrison et al. 1965).

Maximum mass

The TOV equations can be solved exactly for an incompressible star $\rho(r) = \rho_s$. Equation (3.22) can be easily integrated:

$$m(r) = \frac{4}{3}\pi r^3 \rho_s\,. \tag{3.29}$$

Substituting into Eq. (3.21) and integrating leads to

$$P(r) = \rho_s c^2 \frac{\sqrt{1 - \dfrac{2Gm_s}{R_s c^2}} - \sqrt{1 - \dfrac{2Gm(r)}{rc^2}}}{\sqrt{1 - \dfrac{2Gm(r)}{rc^2}} - 3\sqrt{1 - \dfrac{2Gm_s}{R_s c^2}}}\,. \tag{3.30}$$

The pressure is the highest at the center of the star. Setting $m(r) = 0$ in the above equation using Eq. (1.43) yields

$$P(0) = \rho_s c^2 \frac{\sqrt{1-\mathcal{C}} - 1}{1 - 3\sqrt{1-\mathcal{C}}}\,. \tag{3.31}$$

The mass can be also expressed in terms of the compactness as

$$m_s = \left(\frac{c^2\mathcal{C}}{2G}\right)^{3/2} \left(\frac{3}{4\pi\rho_s}\right)^{1/2}. \tag{3.32}$$

Let us recall that the compactness of a Schwarzschild black hole is $\mathcal{C} = 1$. The maximum possible compactness of a star is obtained in

the limit $\frac{P(0)}{\rho_s c^2} \to +\infty$ and is given by $\mathcal{C} = \frac{8}{9}$. This translates into an upper limit on the mass:

$$\boxed{m_{\max} = \frac{4}{9}\left(\frac{c^2}{G}\right)^{3/2} \frac{1}{\sqrt{3\pi\rho_s}} \approx 11.4 \left(\frac{10^{14}\ \mathrm{g\ cm^{-3}}}{\rho_s}\right)^{1/2} M_\odot}. \quad (3.33)$$

Setting $\rho_s = 10^{14}$ g cm^{-3} leads to Zwicky's estimate for the mass of a neutron star of about $11.4 M_\odot$. Whereas the mass (2.20) of an incompressible white dwarf was limited by *special* relativity (through the equation of state), the maximum mass of an incompressible neutron star arises entirely from *general* relativity. Equation (3.33) represents a maximum maximorum because the pressure remains always finite.

A slightly more realistic constraint can be obtained by assuming that $P(0) < \rho_s c^2$. With this condition, the compactness is now limited by $\mathcal{C} < \frac{3}{4}$. This is known as the Buchdahl limit[12]. The corresponding mass is given by

$$\boxed{m_{\text{Buchdahl}} = \frac{9}{32}\left(\frac{c^2}{G}\right)^{3/2} \frac{1}{\sqrt{2\pi\rho_s}} \approx 8.84 \left(\frac{10^{14}\ \mathrm{g\ cm^{-3}}}{\rho_s}\right)^{1/2} M_\odot}. \quad (3.34)$$

The condition $P < \rho c^2$ is certainly satisfied at low enough densities since ρ always contains the mass energy of the baryons. Remarking that $\frac{dP}{d\rho} = c_s^2$, where c_s is the speed of sound and requiring $c_s < c$ (to ensure causality), implies after integration that $P(r) < \rho(r)c^2$ everywhere inside the star. However, the limit (3.34) was obtained under the unrealistic assumption of an incompressible star.

Hermann Bondi[13] showed that $\mathcal{C} < 0.78$ assuming only $\rho(r)c^2 > P(r) > 0$ throughout the star (but without assuming uniform density) leading to

$$\boxed{m_{\text{Bondi}} \approx 9.37 \left(\frac{10^{14}\ \mathrm{g\ cm^{-3}}}{\rho_s}\right)^{1/2} M_\odot}. \quad (3.35)$$

The most compact configurations are obtained when the low-density equation of state is very soft while the high-density equation of state is very stiff[14]. Considering the maximally compact equation of state allowed by causality, namely $P = 0$ if $\rho < \rho_0$ and $P = c^2(\rho - \rho_0)$ otherwise, the compactness is found to be limited by[15] $\mathcal{C} < 0.7081$. This limit does not depend on ρ_0.

As a matter of fact, the equation of state $P(\rho)$ of dense matter is relatively well known up to a few times 10^{14} g cm^{-3} (corresponding to the crust and outer core of a neutron star). Imposing that the equation of state is the stiffest possible $\frac{dP}{d\rho} = c^2$ (causal limit) only

[12] H. A. Buchdahl. General Relativistic Fluid Spheres. *Physical Review*, 116 (4):1027–1034, November 1959. DOI: 10.1103/PhysRev.116.1027. URL https://doi.org/10.1103/PhysRev.116.1027

[13] H. Bondi. Massive spheres in general relativity. *Proceedings of the Royal Society of London. Series A, Mathematical and Physical Sciences*, 282(1390):303–317, 1964. ISSN 00804630. URL http://www.jstor.org/stable/2414776

[14] Clifford E. Rhoades and Remo Ruffini. Maximum Mass of a Neutron Star. *Phys. Rev. Lett.*, 32(6):324–327, February 1974. DOI: 10.1103/PhysRevLett.32.324. URL https://doi.org/10.1103/PhysRevLett.32.324

[15] P. Haensel, J. P. Lasota, and J. L. Zdunik. On the minimum period of uniformly rotating neutron stars. *Astron. Astrophys.*, 344:151–153, April 1999

above some density $\rho_{\max}$ leads to the more stringent upper mass limit[16]:

$$\boxed{m_{\rm causal} \approx 4.8 \left(\frac{2\times 10^{14}\ {\rm g\ cm^{-3}}}{\rho_{\max}}\right)^{1/2} M_\odot}\,. \tag{3.36}$$

Calculations using modern equations of state yield maximum masses[17] in the range $2-2.5M_\odot$.

Theoretical mass-radius relations for different equations of state are plotted in Fig. 3.10. Measurements of neutron-star masses are summarized in Fig. 3.11.

[16] Scott Koranda, Nikolaos Stergioulas, and John L. Friedman. Upper Limits Set by Causality on the Rotation and Mass of Uniformly Rotating Relativistic Stars. *Astrophys. J.*, 488(2):799–806, October 1997. DOI: 10.1086/304714. URL https://doi.org/10.1086/304714

[17] N. Chamel, P. Haensel, J. L. Zdunik, and A. F. Fantina. On the Maximum Mass of Neutron Stars. *International Journal of Modern Physics E*, 22(7):1330018, July 2013. DOI: 10.1142/S0218301331330018X. URL https://doi.org/10.1142/S021830131330018X

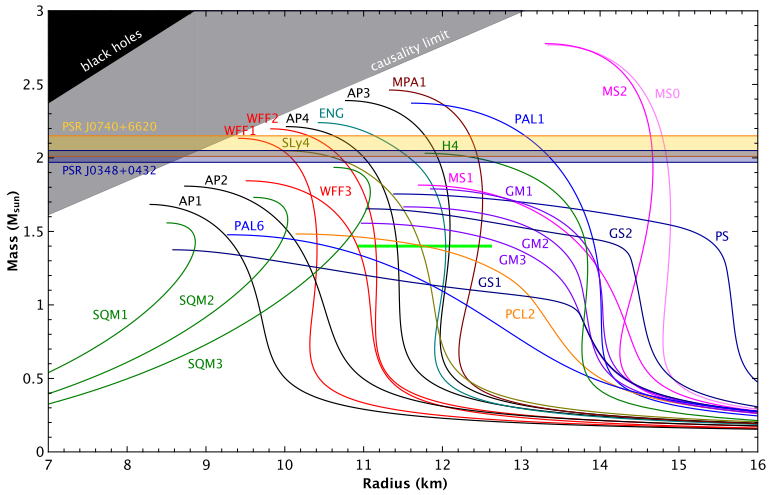

Figure 3.10: Neutron-star masses and radii predicted by different models ("SQM1-3" correspond to hypothetical quark stars). The horizontal lines are 68.3% confidence limits for the two most massive pulsars. The green horizontal bar represents the 90% confidence radius limits from the multi-messenger analysis of Dietrich et al. 2020. Figure created by Norbert Wex.

3.5 *Gravitational-wave detections*

Neutron star inspirals

Several gravitational-wave signals from compact binaries involving at least one neutron star have been detected during their last orbits before merger by ground-based interferometers since 2017.

Considering quasicircular orbits at leading post Newtonian order, the time τ to merger (1.40) can be estimated as

$$\tau \approx 2.18 \left(\frac{1.21M_\odot}{\mathcal{M}}\right)^{5/3} \left(\frac{100{\rm Hz}}{f_{\rm GW}}\right)^{8/3} {\rm s}\,. \tag{3.37}$$

The semimajor axis can be inferred from Kepler's law (1.15)

$$a \approx 1.56\times 10^2 \left(\frac{m}{2.8M_\odot}\right)^{1/3} \left(\frac{100{\rm Hz}}{f_{\rm GW}}\right)^{2/3}\,. \tag{3.38}$$

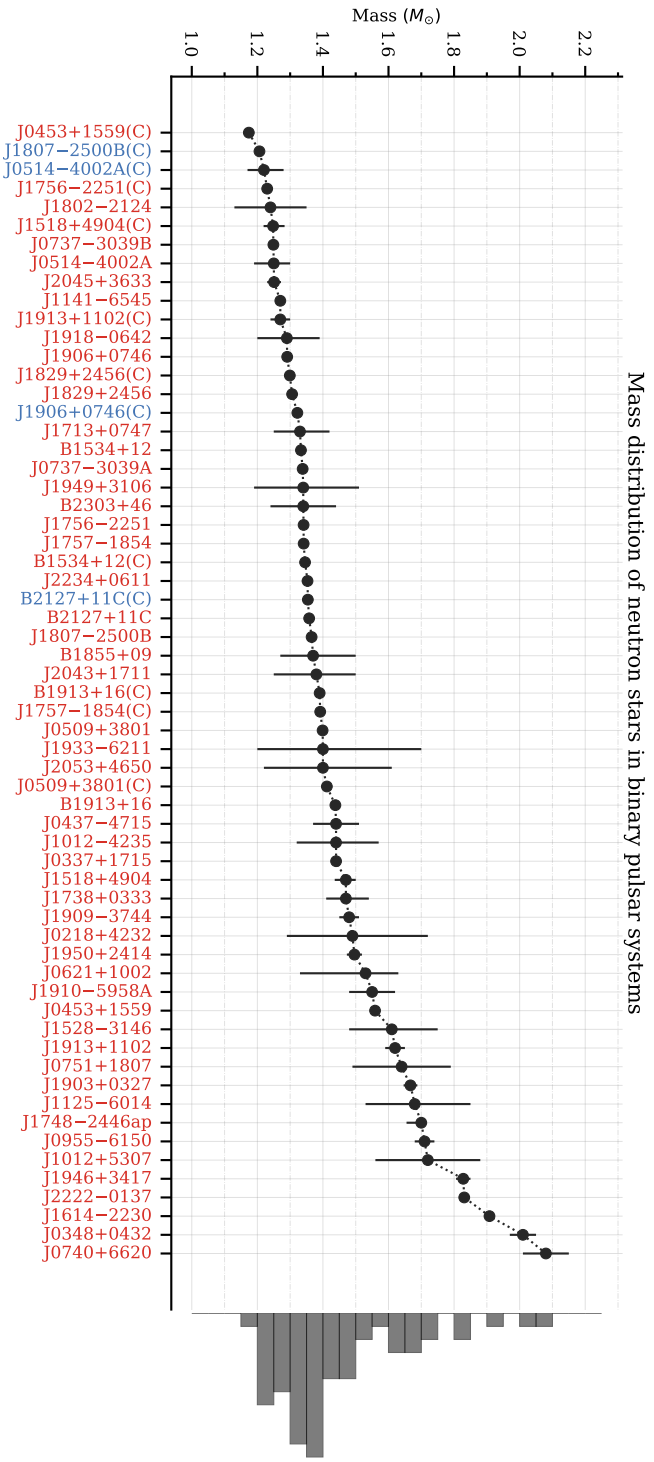

Figure 3.11: Neutron star mass measurements. The letter C in parentheses indicates a companion to a pulsar that is itself not a pulsar. The names in blue are the cases where such a companion could be a neutron star or a massive white dwarf, the names in red are for confirmed neutron stars. The error bars in orange denote multiple recent measurements of the same neutron star mass. The histogram represents the distribution of masses. Figure created by Vivek V. Krishnan.

Typical values for neutron stars are given in Table 3.2.

The frequency marking the end of the inspiral is determined by the innermost stable circular orbit (ISCO) after which the objects plunge and merge. In the test mass limit ($\nu \to 0$, the semimajor axis is $a = \frac{6Gm}{c^2}$ corresponding to

$$f_{\rm GW}^{\rm ISCO} = \frac{1}{6\sqrt{6}\pi}\frac{c^3}{Gm} \approx 4.4\frac{M_\odot}{m}\ {\rm kHz}\,. \tag{3.39}$$

For equal-mass neutron stars with $m_1 = m_2 = 1.4M_\odot$, the frequency is $f_{\rm GW}^{\rm ISCO} \approx 1.6$ kHz corresponding to $\tau = 1.4$ ms before merger. At this point, the orbital separation $a \approx 25$ km is comparable to the size of the neutron stars and their internal structure can no longer be ignored.

$f_{\rm GW}$ (Hz)	τ	a (km)
10	17 min	722
100	2 s	156
1000	4.7 ms	34

Table 3.2: Gravitational-wave frequency $f_{\rm GW}$, time to merger τ and semimajor axis a for the inspiral of equal mass neutron stars with $m_1 = m_2 = 1.4M_\odot$.

The number of gravitational-wave cycles detected between times $t_{\rm min}$ and $t_{\rm max}$ in the frequency window $f_{\rm GW}^{\rm min}$ and $f_{\rm GW}^{\rm max}$ is given by

$$\mathcal{N} = \int_{t_{\rm min}}^{t_{\rm max}} dt f_{\rm GW} = \int_{f_{\rm GW}^{\rm min}}^{f_{\rm GW}^{\rm max}} df_{\rm GW}\frac{f_{\rm GW}}{\dot{f}_{\rm GW}}\,. \tag{3.40}$$

Substituting Eq. (1.34) and considering that $f_{\rm GW}^{\rm min} \ll f_{\rm GW}^{\rm max}$ leads to

$$\mathcal{N} \approx 1.6\times 10^4 \left(\frac{10\ {\rm Hz}}{f_{\rm GW}^{\rm min}}\right)^{5/3}\left(\frac{1.2M_\odot}{\mathcal{M}}\right)^{5/3}\,. \tag{3.41}$$

Ground-based detectors can follow the inspiral of neutron stars for $10^3 - 10^4$ cycles. More generally, in the post Newtonian theory

$$\mathcal{N} = \frac{x^{5/2}}{32\pi\nu}\left(1 + \wp(x) + \wp(x^{3/2}) + \wp(x^2) + \wp(x^{5/2}) + \dots\right)\,, \tag{3.42}$$

where $x = \left(\frac{Gm\omega}{c^3}\right)^{2/3}$ and $\nu = \mu/m$. To track the evolution of the gravitational-wave signal, one has to use templates that can reproduce $\mathcal{N}$ with an error of order 1. This means that corrections up to $\wp(x^{5/2})$ at least, i.e. up to 2.5 PN, have to be included. Corrections up to 4.5 PN have been recently calculated[18].

[18] Luc Blanchet, Guillaume Faye, Quentin Henry, François Larrouturou, and David Trestini. Gravitational-wave phasing of quasicircular compact binary systems to the fourth-and-a-half post-newtonian order. *Phys. Rev. Lett.*, 131:121402, Sep 2023. DOI: 10.1103/PhysRevLett.131.121402. URL https://link.aps.org/doi/10.1103/PhysRevLett.131.121402

Tidal effects

The internal structure of the neutron stars enters the post Newtonian formalism at 5PN order due to tidal interactions. The dominant contribution comes from quadrupolar deformations.

In the Fourier domain, the gravitational-wave signal is given by

$$\widetilde{h}_+(f) = \frac{1}{\pi^{2/3}}\left(\frac{5}{24}\right)^{1/2}\frac{c}{r}\left(\frac{G\mathcal{M}}{c^3}\right)^{5/6}\frac{1}{f^{7/6}}\frac{1+\cos^2 i}{2}e^{\mathrm{i}\Psi(f)}\,, \quad (3.43)$$

$$\widetilde{h}_\times(f) = \frac{1}{\pi^{2/3}}\left(\frac{5}{24}\right)^{1/2}\frac{c}{r}\left(\frac{G\mathcal{M}}{c^3}\right)^{5/6}\frac{1}{f^{7/6}}\cos i\, e^{\mathrm{i}\left(\Psi(f)+\frac{\pi}{2}\right)}\,. \quad (3.44)$$

The phase can be expanded as

$$\Psi(f) = 2\pi f\left(t_c+\frac{r}{c}\right) - \Psi_0 - \frac{\pi}{4} + \frac{3}{128\nu}x^{-5/2} + \ldots + \delta\Psi_{\rm tidal}\,, \quad (3.45)$$

with the tidal correction[19]

$$\delta\Psi_{\rm tidal} = -\frac{117}{256\nu}x^{5/2}\widetilde{\Lambda}\,, \quad (3.46)$$

$$\widetilde{\Lambda} = \frac{16}{13}\frac{(m_1+12m_2)m_1^4\Lambda_1 + (m_2+12m_1)m_2^4\Lambda_2}{(m_1+m_2)^5}\,. \quad (3.47)$$

The factor $\frac{16}{13}$ is introduced such that $\widetilde{\Lambda} = \frac{\Lambda_1+\Lambda_2}{2}$ for $m_1 = m_2$.

Λ_1 and Λ_2 are the dimensionless tidal deformability coefficients of the two stars, and are related to the Love numbers

$$\Lambda_1 = \frac{2}{3}k_{2,1}\left(\frac{R_1c^2}{Gm_1}\right)^5\,, \quad (3.48)$$

where R_1 denotes the neutron-star radius, and similarly for the other neutron star. The Love number characterizes the mass quadrupole

$$Q_{ij} - \frac{2}{3G}k_2R^5\mathscr{E}_{ij}\,, \quad (3.49)$$

induced by the quadrupolar tidal field of the companion $\mathscr{E}_{ij} = c^2\mathscr{R}_{0i0j}$, where $\mathscr{R}_{\mu\nu\rho\sigma}$ is the Riemann tensor.

The Love number k_2 is given by[20]

$$\begin{aligned}k_2 = {}& \frac{\mathcal{C}^5}{20}(1-\mathcal{C})^2\left[2+\mathcal{C}(y_R-1)-y_R\right]\Big\{\mathcal{C}\left[6-3y_R+\frac{3}{2}\mathcal{C}(5y_R-8)\right]\\ &+\frac{\mathcal{C}^3}{2}\left[13-11y_R+\frac{\mathcal{C}}{2}(3y_R-2)+\frac{\mathcal{C}^2}{2}(1+y_R)\right]\\ &+3(1-\mathcal{C})^2\left[2-y_R+\mathcal{C}(y_R-1)\right]\ln(1-\mathcal{C})\Big\}^{-1}\,, \end{aligned} \quad (3.50)$$

where $\mathcal{C}$ is the compactness parameter (1.43) and the quantity $y_R \equiv y(R_s)$ is obtained by integrating the following differential equation[21]

$$r\frac{dy}{dr} + y(r)^2 + F(r)y(r) + Q(r) = 0\,, \quad (3.51)$$

[19] Kent Yagi. Multipole Love relations. *Phys. Rev. D*, 89(4):043011, February 2014. DOI: 10.1103/PhysRevD.89.043011. URL https://doi.org/10.1103/PhysRevD.89.043011

The order of a post Newtonian correction is defined with respect to the leading term. The post Newtonian corrections to the phase can be written as $\frac{3}{128\nu}x^{-5/2}\left(1+\ldots-\frac{39}{2}\widetilde{\Lambda}x^5\right)$. $\delta\Psi_{\rm tidal}$ is therefore a 5PN correction.

[20] T. Hinderer. Tidal Love Numbers of Neutron Stars. *Astrophys. J.*, 677:1216–1220, April 2008. DOI: 10.1086/533487. URL https://doi.org/10.1086/533487; and T. Hinderer, B. D. Lackey, R. N. Lang, and J. S. Read. Tidal deformability of neutron stars with realistic equations of state and their gravitational wave signatures in binary inspiral. *Phys. Rev. D*, 81(12):123016, June 2010. DOI: 10.1103/PhysRevD.81.123016. URL https://doi.org/10.1103/PhysRevD.81.123016

[21] Sergey Postnikov, Madappa Prakash, and James M. Lattimer. Tidal love numbers of neutron and self-bound quark stars. *Phys. Rev. D*, 82:024016, Jul 2010. DOI: 10.1103/PhysRevD.82.024016. URL https://link.aps.org/doi/10.1103/PhysRevD.82.024016

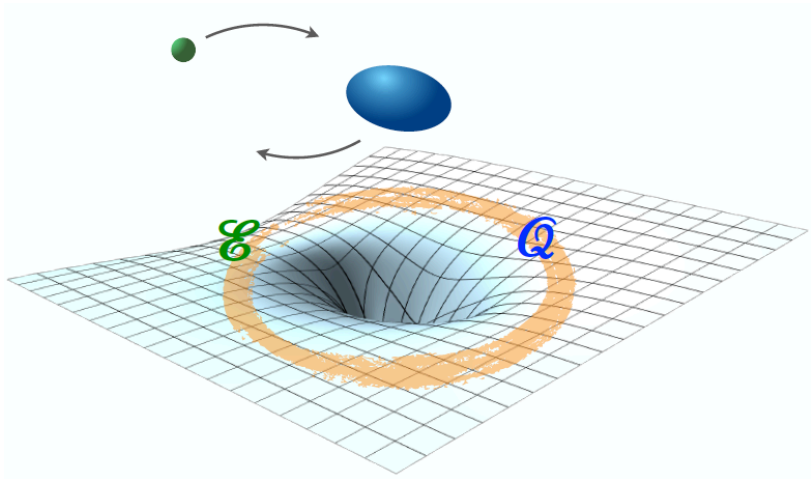

Figure 3.12: Schematic picture illustrating the mass quadrupole of a neutron star induced by the tidal field of a companion. From Dietrich et al. 2021.

$$F(r) = \frac{1 - 4\pi G r^2 (\mathcal{E}(r) - P(r))/c^4}{1 - 2Gm(r)/(rc^2)}, \tag{3.52}$$

$$Q(r) = \frac{4\pi G r^2/c^4}{1 - 2Gm(r)/(rc^2)} \left[5\mathcal{E}(r) + 9P(r) + \frac{\mathcal{E}(r) + P(r)}{c_s(r)^2} c^2 - \frac{6\,c^4}{4\pi r^2 G} \right] - 4 \left[\frac{G(m(r)/(rc^2) + 4\pi r^2 P(r)/c^4)}{1 - 2Gm(r)/(rc^2)} \right]^2. \tag{3.53}$$

Here $\mathcal{E}(r) = \rho(r)c^2$ denotes the energy density at the radial (circumferential) coordinate r, $P(r)$ the pressure, $c_s = c\sqrt{dP/d\mathcal{E}}$ the sound speed, and $m(r)$ is the gravitational mass function obtained from the solution of the TOV equations. Equation (3.51) must be solved with the boundary condition $y(0) = 2$.

Even though $\delta\Psi_{\rm tidal}$ is of order 5PN, its contribution can be comparable to lower order terms in the late inspiral. This is because λ_1 and Λ_2 are quite large of order $10^2 - 10^3$.

Love numbers calculated using realistic equations of state of neutron stars can be found in Perot and Chamel 2021.

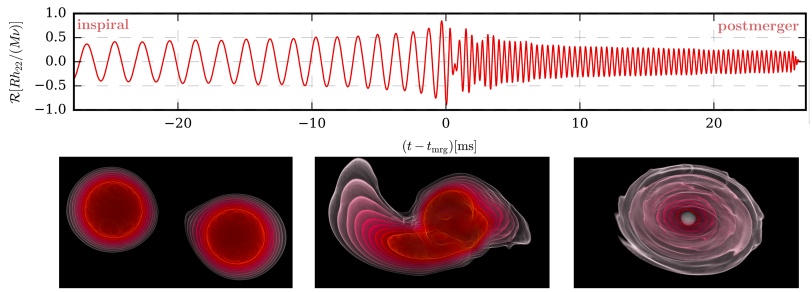

Figure 3.13: Numerical relativity simulation of the inspiral and merger of two neutron stars showing the gravitational-wave signal (top panel) and the matter evolution (bottom panel). From Dietrich et al. 2021.

The first gravitational-wave templates were constructed from post Newtonian calculations only. Modern templates combines analytic calculations with results from numerical relativity simulations for the merger and postmerger, as shown in Fig. 3.13. Current ground-based detectors are mostly sensitive to the inspiral phase at frequency $f_{\rm GW} \sim 100$ Hz. But the merger and postmerger will be observable with third generation gravitational-wave detectors, such as the Einstein Telescope. The analyses of the signals will then be dominated by systematic errors in the gravitational-wave templates.

According to numerical relativity simulations, the merger of two neutron stars can lead to different scenarios, as illustrated in Fig. 3.14:

- prompt collapse to a black hole,
- formation of a differentially rotating *hypermassive* neutron star and collapse to a black hole after about one second,
- formation of a rigidly rotating *supermassive* neutron star and collapse to a black hole after $\sim 1 - 10^4$ seconds,
- formation of a stable neutron star.

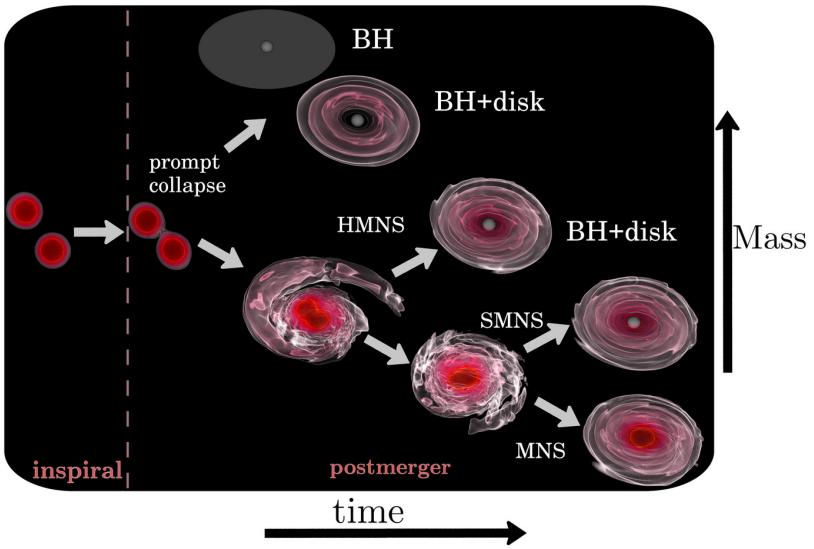

Figure 3.14: Overview about the possible postmerger dynamics and outcome. Mostly depending on the mass (but also the mass ratio and spin), the merger remnant can promptly collapse to ablack hole (BH), otherwise the remnant can be a hypermassive (HMNS) or supermassive (SMNS) neutron star collapsing on a longer timescale to a BH or, if the mass is low enough, it can form a stable neutron star (NS). From Dietrich et al. 2021.

GW170817

The signal was detected by all three LIGO-Hanford, LIGO-Livingston, and Virgo detectors during about 100 seconds in the frequency window 30-400 Hz, see Fig. 3.15. The chirp is clearly visible in the middle panel of this figure. The frequency-time map allowed for a

first estimate of the chirp mass. To leading post Newtonian order, neglecting eccentricy, the chirp mass is given by

$$\mathcal{M} = \frac{c^3}{G}\left(\frac{5}{96}\right)^{3/5} \frac{1}{\pi^{8/5}} \dot{f}_{\rm GW}^{3/5} f_{\rm GW}^{-11/5}. \tag{3.54}$$

The distance could be inferred from the gravitational-wave amplitude $\mathcal{A}$, as follows:

$$r = 4\pi^{2/3} \frac{(G\mathcal{M})^{5/3}}{c^4 \mathcal{A}} f_{\rm GW}^{2/3}. \tag{3.55}$$

Both $\mathcal{M}$ and r could thus be estimated without any gravitational-wave template. Refined values were obtained using match filtering techniques with the purely post Newtonian template for the inspiral referred to as TaylorF2: $\mathcal{M} = 1.188^{0.004}_{0.002} M_\odot$ and $r = 40^{+8}_{-14}$ Mpc. The neutron star masses were estimated as $m_1 = 1.36 - 1.60 M_\odot$ and $m_2 = 1.17 - 1.36 M_\odot$ with a total mass $m = 2.74^{+0.04}_{-0.01} M_\odot$. The tidal deformability was constrained to be $\widetilde{\Lambda} < 800$ at 90% confidence level.

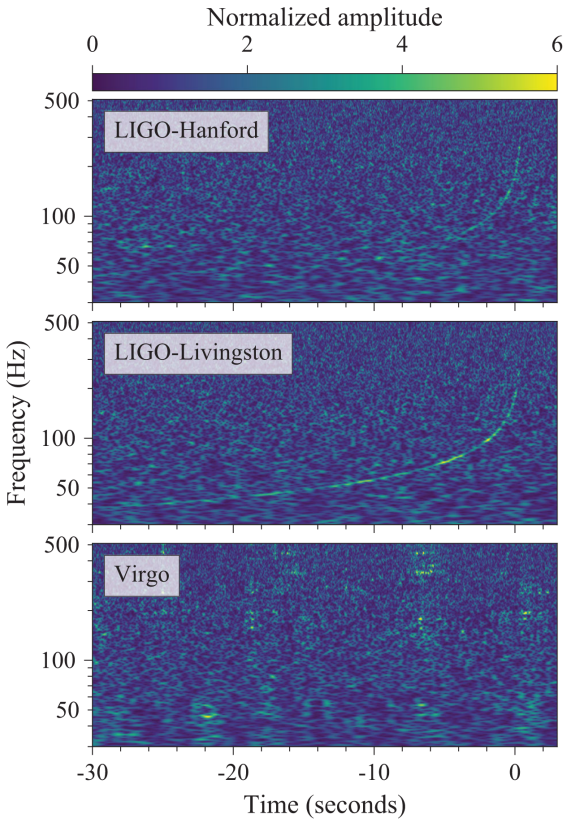

Figure 3.15: Time-frequency representations of data containing the gravitational-wave event GW170817, observed by the LIGO-Hanford (top), LIGO-Livingston (middle), and Virgo (bottom) detectors. Times are shown relative to August 17, 2017 12:41:04 UTC. From LIGO-Virgo scientific collaboration 2017.

The location in the sky was determined by triangulation from differences in the time of arrival as well as the phase and amplitude of the signals received at the different sites. The distance was later

more accurately determined from observations of electromagnetic counterparts.

Subsequent analyses using more realistic gravitational-wave templates for the complete inspiral, merger, and ringdown based on effective one-body methods and numerical relativity led to $\widetilde{\Lambda} = 300^{+420}_{-230}$ assuming low spins, see Fig. 3.16. The rather small value of $\widetilde{\Lambda}$ rules out the stiffest equations of state, and points towards compact neutron stars with comparatively small radii. In particular, the equations of state labelled H4, MS1 and MS1b are found to be incompatible with gravitational-wave data. As shown in Fig. 3.10, these equations of state predict neutron-star radii of about 14 km for $1.4M_\odot$.

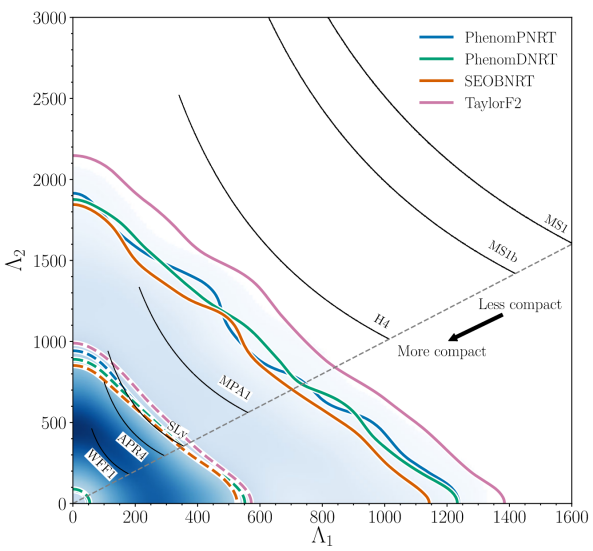

Figure 3.16: Probability density distributions for the tidal deformability parameters Λ_1 and Λ_2 assuming low spins. The blue shading is for the waveform PhenomPNRT. The 50% (dashed lines) and 90% (solid lines) credible regions are shown for the four waveform models. The seven black curves are predictions from different equations of state using the masses estimated with the PhenomPNRT model. From scientific collaboration 2019.

The rather large estimated amount of ejected material $\sim 0.02 - 0.05M_\odot$ inferred from observations and comparison with numerical relativity simulations suggests that the merger remnant did not collapse promptly to a black hole. If this is correct, the total mass m of the binary must be lower than some threshold value approximately given within $0.1M_\odot$ by[22]

$$m_{\rm thres} = m_{\rm max}\left(2.43 - 3.38\frac{Gm_{\rm max}}{R_{\rm max}c^2}\right), \tag{3.56}$$

where $m_{\rm max}$ and $R_{\rm max}$ are the mass and radius of the most massive nonrotating neutron star. Imposing the maximum compactness constraint discussed above

$$\frac{2Gm_{\rm max}}{R_{\rm max}c^2} < 0.7081\,, \tag{3.57}$$

[22] Andreas Bauswein, Oliver Just, Hans-Thomas Janka, and Nikolaos Stergioulas. Neutron-star Radius Constraints from GW170817 and Future Detections. *Astrophys. J. Lett.*, 850(2):L34, December 2017. DOI: 10.3847/2041-8213/aa9994. URL https://doi.org/10.3847/2041-8213/aa9994

leads to

$$m_{\max} < 0.8108 m_{\text{thres}} . \tag{3.58}$$

Setting $m_{\text{thres}} = m$ finally yields an upper limit on the maximum mass of nonrotating neutron stars

$$m_{\max} < 2.22^{+0.03}_{-0.008} M_\odot . \tag{3.59}$$

Substituting into Eq. (3.57) provides a lower bound on the radius:

$$R_{\max} > 9.25^{+0.14}_{-0.03} \text{ km} . \tag{3.60}$$

GW170817 marked the opening of the multimessenger astronomy since this event was also seen across the electromagnetic spectrum by 70 observatories all over the world and in space. A short gamma-ray burst designated GRB 170817A was detected by the Fermi and INTEGRAL satellites 1.7 seconds after the gravitational-wave signal, thus confirming theories according to which such energetic bursts originate from neutron-star mergers. The days and weeks, a transient electromagnetic counterpart referred to as a kilonova designated AT 2017gfo was discovered 11 hours later in the galaxy NGC 4993 and was monitored for days and weeks. Such an emission had been predicted decades earlier from the radioactive decay of ejected materials due to the rapid neutron capture process. The kilonova observation confirmed that heavy elements are produced by neutron-star mergers.

Other gravitational-wave events

Other remarkable gravitational-wave signals from compact binary mergers have been detected by the LIGO-Virgo interferometers.

- GW190425

  The inferred distance is 159^{+69}_{-72} Mpc, the masses of the compact objects are $m_1 = 1.74^{+0.17}_{-0.09} M_\odot$ and $m_2 = 1.56^{+0.08}_{0.14} M_\odot$. No electromagnetic couterpart has been firmly established to this date. The possibility that one or both components are black holes cannot be ruled out.

- GW190814

  This event located at a distance of 241^{+41}_{-45} Mpc involved a black hole with a mass $23.2^{+1.1}_{-1.0} M_\odot$ black hole and a compact object possibly a very massive neutron star with a mass of $2.59^{+0.08}_{-0.09} M_\odot$.

- GW200105

  This event located at a distance of 280^{+110}_{-110} Mpc involved a black hole with a mass $8.9^{+1.2}_{-1.5} M_\odot$ black hole and a compact object likely a neutron star with a mass of $1.9^{+0.3}_{-0.2} M_\odot$.

- GW200115

  This event located at a distance of 300^{+150}_{-100} Mpc involved a black hole with a mass $5.7^{+1.8}_{-2.1} M_\odot$ black hole and a compact object likely a neutron star with a mass of $1.5^{+0.7}_{-0.3} M_\odot$.

- GW230529

  This event located at a distance of 201^{+102}_{-96} Mpc involved a black hole with a mass $3.6^{+0.8}_{-1.2} M_\odot$ black hole and a compact object likely a neutron star with a mass of $1.4^{+0.6}_{-0.2} M_\odot$.

  See https://www.ligo.caltech.edu/page/ligo-publications for references.

  The full list of events detected by the LIGO-Virgo-KAGRA interferometers can be found at https://gwosc.org/.

A
Estimate of the radius of an atom

Let us consider a very simple model of an atom consisting of a positively charge nucleus embedded in a spherical electron cloud of radius a, as illustrated in Fig. A.1. Electrons are treated as a free Fermi gas with density n_e. Since the overall atom is electrically charge neutral, we must have

$$n_e = \frac{3Z}{4\pi a^3}\,. \tag{A.1}$$

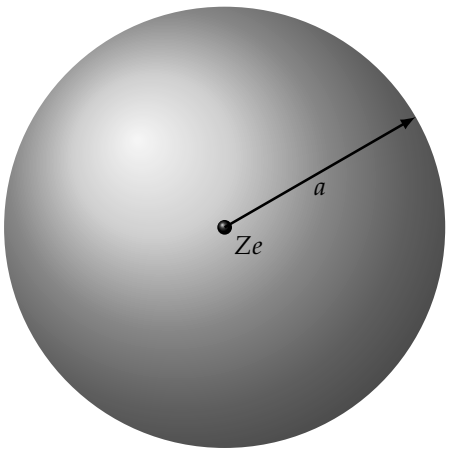

Figure A.1: Simple model of an atom with Z protons contained in the core and Z electrons uniformly distribution in a spherical cloud of radius a.

For the atom to be bound, the kinetic energy of the electron cloud must be compensated by the Coulomb energy. The kinetic energy is given by

$$E_{\rm kin} = \frac{4}{3}\pi a^3 \frac{\hbar^2 k_{Fe}^5}{10\pi^2 m_e}\,, \tag{A.2}$$

with $k_{Fe} = (3\pi^2 n_e)^{1/3}$.

The Coulomb energy $E_{\rm Coul} = E_{e-e} + E_{e-N}$ is due to electron-electron and electron-nucleus interactions. The Coulomb energy of

the uniform cloud of Z electrons is given by

$$E_{e-e} = \int_0^{Ze} \frac{q dq}{r}\,, \tag{A.3}$$

where

$$q = -Ze\left(\frac{r}{a}\right)^3 \tag{A.4}$$

is the charge contained in the electron sphere of radius r. To assemble the electron cloud about the central nucleus of charge Ze requires energy

$$E_{e-N} = Ze\int_0^{a} \frac{dq}{r}\,. \tag{A.5}$$

Carrying out the integrations yields

$$E_{\rm Coul} = -\frac{9}{10}\frac{Z^2e^2}{a}\,. \tag{A.6}$$

Solving $E_{\rm kin} + E_{\rm Coul} = 0$ for a using Eq. (A.1) finally leads to

$$a = \left(\frac{3\pi^2}{16}\right)^{1/3}\frac{a_0}{Z^{1/3}} \sim \frac{a_0}{Z^{1/3}}\,, \tag{A.7}$$

where $a_0 = \dfrac{\hbar^2}{m_e e^2}$ is the Bohr radius.

B
Electron Fermi gas at zero temperature

Let us consider N_e noninteracting electrons of mass m_e contained in a volume V at zero temperature.

B.1 Fermi wave vector

The quantum states of this electron Fermi gas are uniquely determined by the electron wave vector $\vec{k}_e$ and their spin. According to Pauli's principle, electrons cannot occupy the same quantum state. The highest Fermi wave vector k_{Fe} is determined by integrating all occupied states in the Fermi sphere of volume $V_F = \frac{4}{3}\pi k_{Fe}^3$:

$$n_e = \frac{2}{(2\pi)^3}\int_{V_F} d^3k_e = \frac{2}{(2\pi)^3}\int_0^{k_{Fe}} dk_e\, k_e^2 \int_0^{\pi} d\theta \sin\theta \int_0^{2\pi} d\varphi = \frac{k_{Fe}^3}{3\pi^2}\,. \quad \text{(B.1)}$$

The factor of 2 accounts for the two spin states.

B.2 Pressure and chemical potential

The pressure of N_e electrons contained in a volume V with energy E_e is defined by

$$P_e = -\left.\frac{\partial E_e}{\partial V}\right|_{N_e} = -\left.\frac{\partial (E_e/N_e)}{\partial (V/N_e)}\right|_{N_e} = -\frac{d\mathcal{E}_e}{d(1/n_e)} = n_e^2 \frac{d(\mathcal{E}_e/n_e)}{dn_e}\,, \quad \text{(B.2)}$$

where $\mathcal{E}_e = \dfrac{E_e}{V}$ is the energy density and $n_e = \dfrac{N_e}{V}$ is the electron number density.

The chemical potential is given by

$$\mu_e = \left.\frac{\partial E_e}{\partial N_e}\right|_V = \left.\frac{\partial (E_e/V)}{\partial (N_e/V)}\right|_V = \frac{d\mathcal{E}_e}{dn_e}\,. \quad \text{(B.3)}$$

Note that the pressure can be obtained from the Gibbs-Duhem relation

$$P_e = n_e \mu_e - \mathcal{E}_e \,. \tag{B.4}$$

In principle, the pressure and the chemical potential must be calculated at fixed entropy S. This is the case here since $T = 0$ implies $S = 0$ from the third law of thermodynamics.

B.3 Energy density

Non-relativistic limit

The energy of a non-relativistic electron wih momentum $\vec{p}_e$ is given by $\varepsilon_e(\vec{p}_e) = \dfrac{p_e^2}{2m_e}$.

Using the De Brogli relation $\vec{p}_e = \hbar \vec{k}_e$ and integrating over all occupied states yields

$$\mathcal{E}_e = \frac{2}{(2\pi)^3} \int\limits_{V_F} d^3k_e \, \frac{\hbar^2 k_e^2}{2m_e} = \frac{2}{(2\pi)^3} \int\limits_0^{k_{Fe}} dk_e \, k_e^2 \frac{\hbar^2 k_e^2}{2m_e} 4\pi = \frac{\hbar^2 k_{Fe}^5}{10\pi^2 m_e} \,. \tag{B.5}$$

Note that the chemical potential coincides with the Fermi energy

$$\mu_e = \frac{\hbar^2 k_{Fe}^2}{2m_e} \,. \tag{B.6}$$

Ultrarelativistic limit

The energy of a relativistic electron wih momentum $\vec{p}_e$ is given by $\varepsilon_e(\vec{p}_e) = \sqrt{m_e^2 c^4 + p_e^2 c^2}$. In the ultrarelativistic limit $p_e \gg m_e c$, the energy is approximately given by $\varepsilon_e(\vec{p}_e) \approx p_e c$.

Using the De Brogli relation $\vec{p}_e = \hbar \vec{k}_e$ and integrating over all occupied states yields

$$\mathcal{E}_e = \frac{2}{(2\pi)^3} \int\limits_{V_F} d^3k_e \, \hbar c k_e = \frac{2}{(2\pi)^3} \int\limits_0^{k_{Fe}} dk_e \, k_e^2 \hbar c k_e 4\pi = \frac{\hbar c k_{Fe}^4}{4\pi^2} \,. \tag{B.7}$$

Note that the chemical potential coincides with the Fermi energy

$$\mu_e = \hbar c k_{Fe} \,. \tag{B.8}$$

Bibliography

Wilhelm Anderson. Über die Grenzdichte der Materie und der Energie. *Zeitschrift fur Physik*, 56(11-12):851–856, November 1929. DOI: 10.1007/BF01340146. URL https://doi.org/10.1007/BF01340146.

W. Baade and F. Zwicky. Cosmic Rays from Super-novae. *Proceedings of the National Academy of Science*, 20(5):259–263, May 1934. DOI: 10.1073/pnas.20.5.259. URL https://doi.org/10.1073/pnas.20.5.259.

Andreas Bauswein, Oliver Just, Hans-Thomas Janka, and Nikolaos Stergioulas. Neutron-star Radius Constraints from GW170817 and Future Detections. *Astrophys. J. Lett.*, 850(2):L34, December 2017. DOI: 10.3847/2041-8213/aa9994. URL https://doi.org/10.3847/2041-8213/aa9994.

J. Bennett, M. Donahue, N. Schneder, and M. Voit. *The Cosmic Perspective, 8th Edition*. Pearson Addison Wesley, 2017.

Luc Blanchet, Guillaume Faye, Quentin Henry, François Larrouturou, and David Trestini. Gravitational-wave phasing of quasicircular compact binary systems to the fourth-and-a-half post-newtonian order. *Phys. Rev. Lett.*, 131:121402, Sep 2023. DOI: 10.1103/PhysRevLett.131.121402. URL https://link.aps.org/doi/10.1103/PhysRevLett.131.121402.

H. Bondi. Massive spheres in general relativity. *Proceedings of the Royal Society of London. Series A, Mathematical and Physical Sciences*, 282 (1390):303–317, 1964. ISSN 00804630. URL http://www.jstor.org/stable/2414776.

R. A. Brooker and T. W. Olle. Apsidal-Motion Constants for Polytropic Models. *Monthly Notices of the Royal Astronomical Society*, 115(1): 101–106, 02 1955. ISSN 0035-8711. DOI: 10.1093/mnras/115.1.101. URL https://doi.org/10.1093/mnras/115.1.101.

H. A. Buchdahl. General Relativistic Fluid Spheres. *Physical Review*, 116(4):1027–1034, November 1959. DOI: 10.1103/PhysRev.116.1027. URL https://doi.org/10.1103/PhysRev.116.1027.

A. G. Cameron. Neutron Star Models. *Astrophys. J.*, 130:884, November 1959. DOI: 10.1086/146780. URL https://doi.org/10.1086/146780.

N. Chamel, P. Haensel, J. L. Zdunik, and A. F. Fantina. On the Maximum Mass of Neutron Stars. *International Journal of Modern Physics E*, 22(7):1330018, July 2013. DOI: 10.1142/S021830131330018X. URL https://doi.org/10.1142/S021830131330018X.

S. Chandrasekhar. The Maximum Mass of Ideal White Dwarfs. *Astrophys. J.*, 74:81, July 1931. DOI: 10.1086/143324. URL https://doi.org/10.1086/143324.

Tim Dietrich, Tanja Hinderer, and Anuradha Samajdar. Interpreting binary neutron star mergers: describing the binary neutron star dynamics, modelling gravitational waveforms, and analyzing detections. *General Relativity and Gravitation*, 53(3):27, March 2021. DOI: 10.1007/s10714-020-02751-6. URL https://doi.org/10.1007/s10714-020-02751-6.

Tim Dietrich et al. Multimessenger constraints on the neutron-star equation of state and the hubble constant. *Science*, 370(6523): 1450–1453, 2020. DOI: 10.1126/science.abb4317. URL https://www.science.org/doi/abs/10.1126/science.abb4317.

A. S. Eddington. The Internal Constitution of the Stars. *Nature.*, 106(2653):14–20, September 1920. DOI: 10.1038/106014a0. URL https://doi.org/10.1038/106014a0.

A. S. Eddington. *The Internal Constitution of the Stars*. Cambridge University Press, 1926.

Eliot Finch et al. Identifying LISA verification binaries among the Galactic population of double white dwarfs. *Monthly Notices of the Royal Astronomical Society*, 522(4):5358–5373, 04 2023. ISSN 0035-8711. DOI: 10.1093/mnras/stad1288. URL https://doi.org/10.1093/mnras/stad1288.

R. H. Fowler. On dense matter. *Mon. Not. R. Astron. Soc.*, 87:114–122, December 1926. DOI: 10.1093/mnras/87.2.114. URL https://doi.org/10.1093/mnras/87.2.114.

C. Fransson et al. Emission lines due to ionizing radiation from a compact object in the remnant of supernova 1987a. *Science*, 383(6685):898–903, 2024. DOI: 10.1126/science.adj5796. URL https://www.science.org/doi/abs/10.1126/science.adj5796.

Jim Fuller and Dong Lai. Dynamical tides in compact white dwarf binaries: tidal synchronization and dissipation. *Mon. Not. R.*

Astron. Soc., 421(1):426–445, March 2012. DOI: 10.1111/j.1365-2966.2011.20320.x. URL https://doi.org/10.1111/j.1365-2966.2011.20320.x.

P. Haensel, J. P. Lasota, and J. L. Zdunik. On the minimum period of uniformly rotating neutron stars. *Astron. Astrophys.*, 344:151–153, April 1999.

P. Haensel, A. Y. Potekhin, and D. G. Yakovlev. *Neutron Stars. 1. Equation of State and Structure*. Springer, New York, 2007.

B. K. Harrison, M. Wakano, and J. A. Wheeler. Matter-energy at high density: end point of thermonuclear evolution. In *Onzième Conseil de Physique Solvay, Stoops, Brussels*, page 124, 1958.

B. K. Harrison, K. S. Thorne, M. Wakano, and J. A. Wheeler. *Gravitation Theory and Gravitational Collapse*. Chicago: University of Chicago Press, 1965.

J. J. Hermes et al. Rapid Orbital Decay in the 12.75-minute Binary White Dwarf J0651+2844. *Astrophys. J. Lett.*, 757(2):L21, October 2012. DOI: 10.1088/2041-8205/757/2/L21. URL https://doi.org/10.1088/2041-8205/757/2/L21.

T. Hinderer. Tidal Love Numbers of Neutron Stars. *Astrophys. J.*, 677:1216–1220, April 2008. DOI: 10.1086/533487. URL https://doi.org/10.1086/533487.

T. Hinderer, B. D. Lackey, R. N. Lang, and J. S. Read. Tidal deformability of neutron stars with realistic equations of state and their gravitational wave signatures in binary inspiral. *Phys. Rev. D*, 81 (12):123016, June 2010. DOI: 10.1103/PhysRevD.81.123016. URL https://doi.org/10.1103/PhysRevD.81.123016.

S. A. Kaplan. Sverkhplotnyè Zvezdy. *Naukovy Zapiski*, 15:109–115, 1949.

Scott Koranda, Nikolaos Stergioulas, and John L. Friedman. Upper Limits Set by Causality on the Rotation and Mass of Uniformly Rotating Relativistic Stars. *Astrophys. J.*, 488(2):799–806, October 1997. DOI: 10.1086/304714. URL https://doi.org/10.1086/304714.

L. D. Landau. To the Stars theory. *Phys. Zs. Sowjet*, 1:285, December 1932.

LIGO-Virgo scientific collaboration. Gw170817: Observation of gravitational waves from a binary neutron star inspiral. *Phys. Rev. Lett.*, 119:161101, Oct 2017. DOI: 10.1103/PhysRevLett.119.161101. URL https://link.aps.org/doi/10.1103/PhysRevLett.119.161101.

W. J. Luyten. Third Note on Faint Early Type Stars with Large Proper Motion. *Pub. Astr. Soc. P.*, 34(202):356–357, December 1922. DOI: 10.1086/123249. URL https://doi.org/10.1086/123249.

Michele Maggiore. *Gravitational Waves. Vol. 1: Theory and Experiments*. Oxford University Press, 2018a.

Michele Maggiore. *Gravitational Waves. Vol. 2: Astrophysics and Cosmology*. Oxford University Press, 2018b.

A. I. Miller. *Empire of the Stars: Friendship, Obsession and Betrayal in the Quest for Black holes*. Little, Brown Book Group, 2007.

Coleman Miller and Nicolás Yunes. *Gravitational Waves in Physics and Astrophysics: An Artisan's Guide*. Institute of Physics Publishing, 2021.

Simon Mitton. *The Crab Nebula*. Charles Scribner's sons, 1979.

J. R. Oppenheimer and Robert Serber. On the Stability of Stellar Neutron Cores. *Physical Review*, 54(7):540–540, October 1938. DOI: 10.1103/PhysRev.54.540. URL https://doi.org/10.1103/PhysRev.54.540.

J. R. Oppenheimer and G. M. Volkoff. On Massive Neutron Cores. *Physical Review*, 55(4):374–381, February 1939. DOI: 10.1103/PhysRev.55.374. URL https://doi.org/10.1103/PhysRev.55.374.

Abraham Pais. *Inward bound. Of matter and forces in the physical world*. Oxford University Press, 1986.

L. Perot and N. Chamel. Role of dense matter in tidal deformations of inspiralling neutron stars and in gravitational waveforms with unified equations of state. *Phys. Rev. C*, 103(2):025801, February 2021. DOI: 10.1103/PhysRevC.103.025801. URL https://doi.org/10.1103/PhysRevC.103.025801.

L. Perot and N. Chamel. Tidal deformability of crystallized white dwarfs in full general relativity. *Phys. Rev. D*, 106(2):023012, July 2022. DOI: 10.1103/PhysRevD.106.023012. URL https://doi.org/10.1103/PhysRevD.106.023012.

P. C. Peters and J. Mathews. Gravitational Radiation from Point Masses in a Keplerian Orbit. *Physical Review*, 131(1):435–440, July 1963. DOI: 10.1103/PhysRev.131.435. URL https://doi.org/10.1103/PhysRev.131.435.

Sergey Postnikov, Madappa Prakash, and James M. Lattimer. Tidal love numbers of neutron and self-bound quark stars. *Phys. Rev. D*, 82:024016, Jul 2010. DOI: 10.1103/PhysRevD.82.024016. URL https://link.aps.org/doi/10.1103/PhysRevD.82.024016.

Clifford E. Rhoades and Remo Ruffini. Maximum Mass of a Neutron Star. *Phys. Rev. Lett.*, 32(6):324–327, February 1974. DOI: 10.1103/PhysRevLett.32.324. URL https://doi.org/10.1103/PhysRevLett.32.324.

E. Schatzman. Influence of the Nucleon-Electron Equilibrium on the Internal Structure of White Dwarfs. *Astronomiceskij Zhurnal*, 1956.

Evry Schatzman. *White Dwarfs*. North-Holland Publishing Company, 1958.

LIGO-Virgo scientific collaboration. Properties of the binary neutron star merger gw170817. *Phys. Rev. X*, 9:011001, Jan 2019. DOI: 10.1103/PhysRevX.9.011001. URL https://link.aps.org/doi/10.1103/PhysRevX.9.011001.

Stuart L. Shapiro and Saul A. Teukolsky. *Black holes, white dwarfs and neutron stars. The physics of compact objects*. John Wiley and Sons, 1983.

T. E. Sterne. Apsidal Motion in Binary Stars. *Monthly Notices of the Royal Astronomical Society*, 99(5):451–462, 03 1939. ISSN 0035-8711. DOI: 10.1093/mnras/99.5.451. URL https://doi.org/10.1093/mnras/99.5.451.

E. C. Stoner. The minimum pressure of a degenerate electron gas. *Monthly Notices of the Royal Astronomical Society*, 92(7):651–661, 05 1932. ISSN 0035-8711. DOI: 10.1093/mnras/92.7.651. URL https://doi.org/10.1093/mnras/92.7.651.

Edmund C. Stoner. V. the limiting density in white dwarf stars. *The London, Edinburgh, and Dublin Philosophical Magazine and Journal of Science*, 7(41):63–70, 1929. DOI: 10.1080/14786440108564713. URL https://doi.org/10.1080/14786440108564713.

Edmund C. Stoner. Lxxxvii. the equilibrium of dense stars. *The London, Edinburgh, and Dublin Philosophical Magazine and Journal of Science*, 9(60):944–963, 1930. DOI: 10.1080/14786443008565066. URL https://doi.org/10.1080/14786443008565066.

Kip S. Thorne. *Black holes and time warps: Einstein's outrageous legacy*. 1994.

F. Valsecchi, W. M. Farr, B. Willems, C. J. Deloye, and V. Kalogera. Tidally Induced Apsidal Precession in Double White Dwarfs: A New Mass Measurement Tool with LISA. *Astrophys. J.*, 745(2):137, February 2012. DOI: 10.1088/0004-637X/745/2/137. URL https://doi.org/10.1088/0004-637X/745/2/137.

Tucker Wallace and Riccardo Giacconi. *The X-ray Universe*. Harvard University Press, 1985.

Linqing Wen. On the eccentricity distribution of coalescing black hole binaries driven by the kozai mechanism in globular clusters. *The Astrophysical Journal*, 598(1):419, nov 2003. DOI: 10.1086/378794. URL https://dx.doi.org/10.1086/378794.

S. E. Woosley, A. Heger, and T. A. Weaver. The evolution and explosion of massive stars. *Reviews of Modern Physics*, 74(4):1015–1071, November 2002. DOI: 10.1103/RevModPhys.74.1015. URL https://doi.org/10.1103/RevModPhys.74.1015.

Kent Yagi. Multipole Love relations. *Phys. Rev. D*, 89(4):043011, February 2014. DOI: 10.1103/PhysRevD.89.043011. URL https://doi.org/10.1103/PhysRevD.89.043011.

Dmitrii G. Yakovlev. From the history of physics: The article by Ya I Frenkel' on 'binding forces' and the theory of white dwarfs. *Physics Uspekhi*, 37(6):609–612, June 1994. DOI: 10.1070/PU1994v037n06ABEH000031. URL https://doi.org/10.1070/PU1994v037n06ABEH000031.

Dmitrii G. Yakovlev, Pawel Haensel, Gordon Baym, and Christopher Pethick. Lev Landau and the concept of neutron stars. *Physics Uspekhi*, 56(3):289-295, March 2013. DOI: 10.3367/UFNe.0183.201303f.0307. URL https://doi.org/10.3367/UFNe.0183.201303f.0307.

F. Zwicky. On Collapsed Neutron Stars. *Astrophys. J.*, 88:522–525, November 1938. DOI: 10.1086/144003. URL https://doi.org/10.1086/144003.

Index

ÉVALUATION
DES ENSEIGNEMENTS
PAR LES ÉTUDIANTS

ULB

ÉVALUATION DES ENSEIGNEMENTS

Dès le quadrimestre terminé, évaluez vos enseignements

Pour :
- **Donner une rétroaction à vos enseignants**
- **Proposer des améliorations**
- **Participer à l'évolution des enseignements**
- **Valoriser les activités d'enseignement**

Une évaluation à plusieurs dimensions

Portant sur :
- **La conception de l'enseignement**
- **Le déroulement des séances**
- **L'évaluation des apprentissages (examen)**
- **La prestation des enseignants**

VOTRE AVIS COMPTE !

→ https://www.ulb.be/fr/qualite/l-evaluation-des-enseignements-par-les-etudiants

L'évaluation institutionnelle des enseignements est organisée par l'ULB.
Elle a lieu dès que les enseignements sont terminés. Elle se déroule en deux campagnes d'enquête en ligne après les sessions de janvier et de juin.

L'étudiant répond anonymement à un questionnaire pour chaque enseignement auquel il a participé. Chaque questionnaire est analysé et les résultats sont envoyés aux enseignants et à la commission pédagogique facultaire.

La participation de l'ensemble des étudiants et des enseignants est indispensable pour l'amélioration des programmes

Le label FSC : la garantie d'une gestion responsable des forêts
Les Presses Universitaires de Bruxelles s'engagent !

Les PUB impriment depuis de nombreuses années les syllabus sur du papier recyclé. Les différences de qualité constatées au niveau des papiers recyclés ont cependant poussé les PUB à se tourner vers un papier de meilleure qualité et surtout porteur du label FSC.

Sensibles aux objectifs du FSC et soucieuses d'adopter une démarche responsable, les PUB se sont conformé aux exigences du FSC et ont obtenu en avril 2010 la certification FSC (n° de certificat COC spécifique aux PUB : SCS-COC-005219-HA

Seule l'obtention de ce certificat autorise les PUB à utiliser le label FSC selon des règles strictes. Fortes de leur engagement en faveur de la gestion durable des forêts, les PUB souhaitent dorénavant imprimer tous les syllabus sur du papier certifié FSC. Le label FSC repris sur les syllabus vous en donnera la garantie.

Qu'est-ce que le FSC ?

FSC signifie "Forest Stewardship Council" ou "Conseil de bonne gestion forestière". Il s'agit d'une organisation internationale, non gouvernementale, à but non lucratif qui a pour mission de promouvoir dans le monde une gestion responsable et durable des forêts.
Se basant sur dix principes et critères généraux, le FSC veille à travers la certification des forêts au respect des exigences sociales, écologiques et économiques très poussées sur le plan de la gestion forestière.

Quelles garanties ?

Le système FSC repose également sur la traçabilité du produit depuis la forêt certifiée dont il est issu jusqu'au consommateur final. Cette traçabilité est assurée par le contrôle de chaque maillon de la chaîne de commercialisation/transformation du produit (Chaîne de Contrôle : Chain of Custody – COC). Dans le cas du papier et afin de garantir cette traçabilité, aussi bien le producteur de pâte à papier que le fabricant de papier, le grossiste et l'imprimeur doivent être contrôlés.
Ces contrôles sont effectués par des organismes de certification indépendants.

Les 10 principes et critères du FSC

1. L'aménagement forestier doit respecter les lois nationales, les traités internationaux et les principes et critères du FSC.
2. La sécurité foncière et les droits d'usage à long terme sur les terres et les ressources forestières doivent être clairement définis, documentés et légalement établis.
3. Les droits légaux et coutumiers des peuples indigènes à la propriété, à l'usage et à la gestion de leurs territoires et de leurs ressources doivent être reconnus et respectés.
4. La gestion forestière doit maintenir ou améliorer le bien-être social et économique à long terme des travailleurs forestiers et des communautés locales.
5. La gestion forestière doit encourager l'utilisation efficace des multiples produits et services de la forêt pour en garantir la viabilité économique ainsi qu'une large variété de prestations environnementales et sociales.
6. Les fonctions écologiques et la diversité biologique de la forêt doivent être protégées.
7. Un plan d'aménagement doit être écrit et mis en œuvre. Il doit clairement indiquer les objectifs poursuivis et les moyens d'y parvenir.
8. Un suivi doit être effectué afin d'évaluer les impacts de la gestion forestière.
9. Les forêts à haute valeur pour la conservation doivent être maintenues (par ex : les forêts dont la richesse biologique est exceptionnelle ou qui présentent un intérêt culturel ou religieux important). La gestion de ces forêts doit toujours être fondée sur un principe de précaution.
10. Les plantations doivent compléter les forêts naturelles, mais ne peuvent pas les remplacer. Elles doivent réduire la pression exercée sur les forêts naturelles et promouvoir leur restauration et leur conservation. Les principes de 1 à 9 s'appliquent également aux plantations.

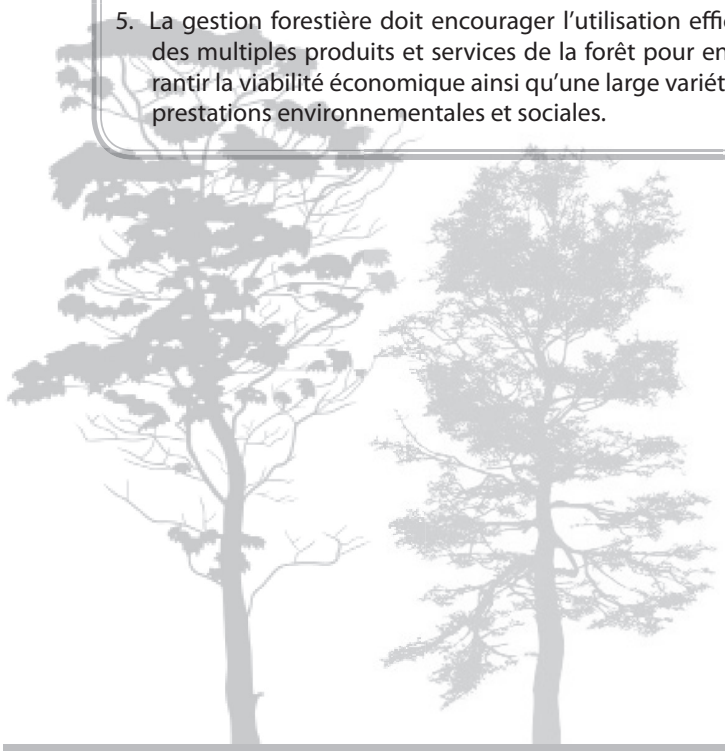

FSC®

Le label FSC apposé sur des produits en papier ou en bois apporte la garantie que ceux-ci proviennent de forêts gérées selon les principes et critères FSC.

® FSC A.C. FSC-SECR-0045

FSC, le label du bois et du papier responsable

Plus d'informations ?
www.fsc.be
A la recherche de produits FSC ?
www.jecherchedufsc.be